Impact of Phase-Shift Error on the Secrecy Performance of Uplink RIS Communication Systems

Abdelhamid Salem, *Member, IEEE*, Kai-Kit Wong, *Fellow, IEEE*, and Chan-Byoung Chae, *Fellow, IEEE*

Abstract—Reconfigurable intelligent surface (RIS) has been recognized as a promising technique for the sixth generation (6G) of mobile communication networks. The key feature of RIS is to reconfigure the propagation environment via smart signal reflections. In addition, active RIS schemes have been recently proposed to overcome the deep path loss attenuation inherent in the RIS-aided communication systems. Accordingly, this paper considers the secrecy performance of up-link RIS-aided multiple users multiple-input single-output (MU-MISO) communication systems, in the presence of multiple passive eavesdroppers. In contrast to the existing works, we investigate the impact of the RIS phase shift errors on the secrecy performance. Taking into account the complex environment, where a general Rician channel model is adopted for all the communication links, closed-form approximate expressions for the ergodic secrecy rate are derived for three RIS configurations, namely, i) passive RIS, ii) active RIS, iii) active RIS with energy harvesting (EH RIS). Then, based on the derived expressions, we optimize the phase shifts at the RIS to enhance the system performance. In addition, the best RIS configuration selection is considered for a given target secrecy rate and amount of the power available at the users. Finally, Monte-Carlo simulations are provided to verify the accuracy of the analysis, and the impact of different system parameters on the secrecy performance is investigated. The results in this paper show that, an active RIS scheme can be implemented to enhance the secrecy performance of RIS-aided communication systems with phase shift errors, especially when the users have limited transmission power.

Index Terms—Reconfigurable intelligent surface, Physical layer security, MU-MISO, MRC.

I. Introduction

Reconfigurable intelligent surface (RIS), also known as intelligent reflecting surface (IRS), has been proposed recently as a promising technique to extend the coverage and improve the spectral efficiency of wireless communication networks [1], [2]. Specifically, RIS is composed of reflecting elements, each of which independently imposes a phase shift on the incident signals. By tuning the phase shifts of the reflecting elements, RIS can convert the propagation environments into smart ones and thus enhance the received signals quality [1], [2]. Due to these advantages, RIS techniques have been extensively considered in the literature. For instance, in [3], the fundamental capacity limit of RIS-aided multiple-input multiple output (MIMO) communication systems has been considered. The achievable ergodic rate of a RIS-assisted MIMO system which comprises links of a Rician channel was derived in [4]. In [5], a closed-form asymptotic ergodic sum rate of a RIS-assisted MIMO communication system was derived under the assumption that the number of base station (BS) antennas tends to infinity. In [6], the up-link achievable rate in RIS-aided massive MIMO systems has been analyzed and optimized. In [7], a closed-form expression of ergodic achievable rate for RIS-aided massive MIMO systems with zero forcing (ZF) detector has been derived. In addition, a closed-form analytical expression for the symbol error probability and the upper bound on the channel capacity of a RIS communication system have been derived in [8]. The ergodic capacity of RIS MIMO networks over Rayleigh-Rician channels was considered in [9].

Nevertheless, the practical implementation of passive RIS-aided communication systems may face several challenges. For instance, the transmitted signal propagates through the RIS experiences a double-fading attenuation, e.g, source-RIS and RIS-destination links. The double-fading attenuation characteristics of RIS were validated through experimental measurements in [10], [11]. This issue has been tackled in the literature by increasing the number of passive RIS elements [12]. However, this solution leads to an increase in the size of the RIS module, which is impractical in some scenarios. To tackle this issue the authors in [13] proposed RIS with active elements. The main idea of active RIS is to adjust the phase shifts and also amplify the reflected signal attenuated from the first link with extra power consumption. A theoretical comparison between the active RIS-assisted communication system and the passive RIS-aided communication system has been presented in [14]. The results in [14] show that active RIS has better performance than passive RIS. The use of active

Abdelhamid Salem is with the department of Electronic and Electrical Engineering, University College London, London, UK, (emails: a.salem@ucl.ac.uk). Abdelhamid Salem is also affiliated with Benghazi University, Benghazi, Libya.

Kai-Kit Wong is with the department of Electronic and Electrical Engineering, University College London, London, UK, (email: kai-kit.wong@ucl.ac.uk). Kai-Kit Wong is also affiliated with Yonsei University, Seoul, Korea.

Chan-Byoung Chae is with Yonsei University, Seoul, Korea (e-mail: cbchae@yonsei.ac.kr).

RIS elements to overcome the double-fading problem has been also investigated in [15], where the results illustrated that using active elements results in a severe reduction in the physical size of RIS to achieve a certain performance. To reduce the power consumption of active RIS, a sub-connected architecture has been proposed in [16]. The energy efficiency in an active RIS-aided multiple users multiple-input single output (MU-MISO) communication system has been investigated in [17].

Although fixed embedded batteries can be used to power the RIS, these batteries cannot be relied on for long time and uninterrupted operations. In addition, wired charging might not be possible to use if the RIS is deployed in inaccessible places. Therefore, equipping RIS elements with energy harvesting (EH) modules can solve these issues. Accordingly, a self-sustainable RIS approach was proposed and studied in the resent researches on RIS. In this regard, in [18] time switching (TS) and power splitting (PS) EH protocols for the RIS to harvest sufficient amount of energy from an access point have been proposed and investigated. The work in [19] considered a self-sustainable RIS-aided MU-MISO communication systems, in which the RIS collected energy from the radio frequency (RF) transmitter using the PS protocol. In [20], a novel transmission policy for a communication network assisted by self-sustainable RIS has been proposed, where the RIS harvests energy from an energy transmitter to support its operation. In [21], self-sustainable RIS with the PS protocol to assist broadcasting network was studied. In [22], self-sustainable RIS-aided communication between a gateway and a device was studied, in which the RIS harvested energy prior communication.

However, most of the aforementioned works on RIS-aided communication systems considered perfect phase shifts design, which is an unrealistic assumption due to the imperfection of the RIS. Practically, phase shift error occurs due to the deviation and inaccuracy of the phase shifts at the RIS elements. Phase shift errors can be caused by various factors such as manufacturing imperfections, calibration inaccuracies, environmental changes, and electronic noise. This error leads to sub-optimal performance of the RIS communication systems. The impact of phase shift errors on the performance of RIS aided communication networks was studied in several works in the literature [23]–[28]. The authors in [23] considered the transmission through a large RIS with phase errors due to imperfect reflectors, and the average error probability was analyzed. The ergodic capacity of RIS-assisted communication systems with phase errors was investigated in [24]. In [25], [26] the achievable rate of RIS-assisted multiple users up-link massive MIMO system under Rician fading channels and with phase errors has been analyzed. The work in [27] considered the impact of hardware impairments on a general RIS MU-MISO system with Rayleigh fading channels. The average achievable rate and optimal phase shifts in the RIS-aided communication systems with hardware impairments at the RIS have been investigated in [28].

A critical challenge that arises with RIS-aided wireless communication systems under imperfect reflectors relates to the information security. The imperfect reflection of the messages makes them prone to eavesdropping because the sub-optimal design of the RIS can cause information leakage to the external eavesdroppers in the system. This implicates vulnerabilities in the signaling security. For the provision of secure transmission, physical layer security (PHYSec) has been proposed from the information theory perspective [29]–[31]. PHYSec exploits the nature of wireless channels to enhance the system security [29]–[31]. PHYSec of RIS systems has also been studied in the literature. In [32], the secrecy throughput maximization problem has been formulated and solved to enhance the secrecy performance of the RIS-assisted MIMO systems. In [33], a novel active RIS design to enhance the security of wireless transmission was proposed. PHYSec of RIS-aided wireless networks has been considered in [34] to achieve secure transmission between a source and a legitimate user in the presence of a malicious eavesdropper. In [35], RIS has been used to perform secure transmission from a multiple antennas transmitter to a multiple antennas legitimate receiver. Further work in [36] considered the secrecy transmission in a RIS-aided multiple antenna communication, where the secrecy rate was improved by optimizing the RIS location. In [37], an active RIS-aided multiple antennas PHYSec transmission scheme was considered, where the active RIS was designed to amplify the signal actively. Recently, the secrecy performance of RIS communication systems under RIS hardware impairments has been analyzed. The secrecy performance of large-RIS-assisted single input single output (SISO) wireless communication systems in the presence of a single eavesdropper and phase errors at the RIS was considered in [38]. Secure beamforming based on deep reinforcement learning was designed in [39] to enhance the secrecy rate of RIS-assisted multiple users full-duplex communication systems with hardware impairments.

Accordingly, this paper investigates the impact of phase shift error on the secrecy performance of up-link RIS-aided MU-MISO systems in the presence of multiple eavesdroppers. The BS receives the users messages only through the RIS, while eavesdroppers can receive the signals from both the direct and reflected links. Applying maximum ration combining (MRC) at the BS, and under Rician fading channels and phase shift errors, the ergodic secrecy rate is analyzed for three RIS configurations, namely, 1) passive RIS, 2) active RIS, and 3) EH RIS. Based on the derived rate expressions, the phase shifts at the RIS are optimized to enhance the system performance. Thus, our system design is based on the two timescale design, where the decoding at the BS is obtained by using the effective channels, while the phase shift is designed based on the long-term statistical channel state information (CSI). Then, the best RIS configuration selection is considered based on the target secrecy rate and amount of power available at the users.

To the best of our knowledge, the impact of the phase

shift errors on the security of RIS-aided up-link communications with different RIS types has not been comprehensively studied in the literature. Thus, to fill this gap we concentrate on the up-link scenario. In addition, the security of the up-link scenario is more crucial because in downlink the BS can exploit the multiple antennas to improve the security. For instance, the BS can employ secure active beamforming, and/or inject artificial noise/jamming signals into the transmitted signals to confuse/jam the eavesdroppers. Also, the available transmit power at the BS is much more than that at the users[1]. For clarity we list the main contributions of this work as follows:

1) We investigate the impact of RIS phase shift error on the secrecy performance of up-link MU-MIMO systems in the presence of multiple passive eavesdroppers.

2) New closed-form explicit analytical expressions for the ergodic secrecy rate are derived for the RIS-assisted MU-MIMO systems, when the RIS is passive, active and EH node under Rician fading channels. This channel model is more general but also very challenging to be considered mathematically. The derived secrecy rate expressions are simple, explicit and in closed form, and provide several important practical design insights.

3) Based on the derived expressions, a genetic algorithm (GA)-based approach is used to obtain the optimal phase shifts. Also, a simple suboptimal technique is proposed to enhance the secrecy rate for a legitimate user.

4) Given a target secrecy rate, we calculate the required user power, and we present steps to select best RIS configuration which depend mainly on the available power at the users.

5) Finally, Monte-Carlo simulations are performed to validate the analytical expressions. The results show that active RIS is an efficient scheme to achieve secure communication in the presence of phase shift errors at the RIS, especially when there is no sufficient amount of power at the users. In addition, increasing number of BS antennas, RIS elements, and the concentration parameter of the phase error, lead to enhance the secrecy performance of up-link RIS communication systems. Furthermore, the RIS should be located close to the users to provide the best secrecy performance.

Next, Section II presents the RIS-aided uplink MU-MISO system model. In Section III, we derive the ergodic secrecy rate of the passive RIS model. Section IV presents the ergodic secrecy rate of the active RIS scheme. Section V derives the ergodic secrecy rate of the EH RIS scheme. Section VIII depicts our numerical results. Our main conclusions are summarized in Section IX.

II. SYSTEM MODEL

Consider a typical up-link RIS-aided MU-MISO communication system consisting of a multiple antennas BS,

---

[1]The downlink scenario will be considered in future work in order to provide a comprehensive study.

an RIS and K single-antenna users in the presence of J single antenna passive eavesdroppers. The BS is equipped with N antennas, and the RIS is equipped with M reflecting elements, as shown in Fig. 1.
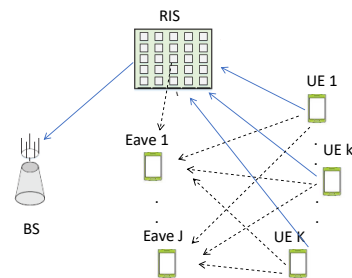

Figure 1: An RIS-aided uplink MU-MISO system with N BS antennas, M RIS elements, K users and J eavesdroppers.

The BS and RIS are connected to control and adjust the phase shifts of the the RIS elements. It is assumed that the eavesdroppers can hear the signals from the direct and reflected links, and trying to eavesdrop a specific confidential message in the system. On the other side, the direct links between the users and BS are assumed to be blocked, which justifies the use of the RIS. It is known that the RIS is most likely to be installed on the buildings, and thus it can create channels dominated by line-of-sight (LoS) path along with scatters. Accordingly, a Rician fading model is considered for the RIS channels. The channel matrix between the RIS and the BS is denoted by $\mathbf{G} \in C^{N \times M}$, and the channel vector between user i and the RIS is presented by $\mathbf{h}_{r,i} \in C^{M \times 1}$. The mathematical expressions of the channel matrix $\mathbf{G}$ and the channel vector $\mathbf{h}_{r,i}$ can be expressed, respectively, as

$$\mathbf{G} = \left(\sqrt{\frac{\rho_b}{\rho_b+1}} \bar{\mathbf{G}} + \sqrt{\frac{1}{\rho_b+1}} \tilde{\mathbf{G}} \right),$$

$$\mathbf{h}_{r,i} = \left(\sqrt{\frac{\rho_i}{\rho_i+1}} \bar{\mathbf{h}}_{r,i} + \sqrt{\frac{1}{\rho_i+1}} \tilde{\mathbf{h}}_{r,i} \right) \quad (1)$$

where ρ_b and ρ_i are the Rician factors, $\bar{\mathbf{G}}$ and $\bar{\mathbf{h}}_{r,i}$ are the LoS components and $\tilde{\mathbf{G}}$ and $\tilde{\mathbf{h}}_{r,i}$ are the NLoS components, in which

$$\bar{\mathbf{G}} = \mathbf{a}_N \left(\phi_r^a, \phi_r^e \right) \mathbf{a}_M^H \left(\phi_t^a, \phi_t^e \right), \bar{\mathbf{h}}_{r,i} = \mathbf{a}_M \left(\phi_{ir}^a, \phi_{ir}^e \right) \quad (2)$$

where ϕ_{ir}^a, ϕ_{ir}^e denote the azimuth and elevation angles of arrival (AoA) from user i to the RIS , respectively, ϕ_t^a, ϕ_t^e are the azimuth and elevation angles of departure (AoD) at the BS from the RIS, respectively, ϕ_r^a, ϕ_r^e are the azimuth and elevation AoA from the RIS to the BS, respectively. The kth element of the vector $\mathbf{a}_X \left(\phi_1, \phi_2 \right)$ can be written as $\left[\mathbf{a}_X \left(\phi_1, \phi_2 \right) \right]_k = e^{j2\pi \frac{d}{\lambda} \left(\tilde{x}_k \sin \phi_1 \sin \phi_2 + \tilde{y}_k \cos \phi_2 \right)}$, where λ is the wavelength, d is the elements/antennas spacing,

and $\tilde{x}_k = (k-1) \bmod \sqrt{X}$, $\tilde{y}_k = \frac{k-1}{\sqrt{X}}$. On the other hand, the channel vector between the RIS and eavesdropper j is presented by $\mathbf{h}_{e_j,r} \in C^{1 \times M}$, and the channel from user i to eavesdropper j is $h_{e_j,i} \in C^{1 \times 1}$. The direct channel fading is assumed to be Rayleigh fading due to extensive scatterers, while for the RIS-related channels, is assumed to be Rician fading. Thus the expression of $\mathbf{h}_{e_j,r}$ is given by

$$\mathbf{h}_{e_j,r} = \left(\sqrt{\frac{\rho_{e_j,r}}{\rho_{e_j,r}+1}} \bar{\mathbf{h}}_{e_j,r} + \sqrt{\frac{1}{\rho_{e_j,r}+1}} \tilde{\mathbf{h}}_{e_j,r} \right) \quad (3)$$

where $\rho_{e_j,r}$ is the Rician factor, $\bar{\mathbf{h}}_{e_j,r}$ and $\tilde{\mathbf{h}}_{e_j,r}$ are the LoS of NLoS components, respectively.

The channel state information (CSI) of the eavesdroppers is assumed to be unknown at the BS/RIS (only statistical information can be known), and the eavesdroppers are non-colluding and trying to eavesdrop a specific confidential user's message, user k, in the system. Therefore, the ergodic secrecy rate can be calculated by [40]

$$\hat{R}_s = \left[\hat{R}_{b_k} - \hat{R}_{e_j,k} \right]^+ \quad (4)$$

where $[l]^+ = \max(0, l)$, $\hat{R}_{b_k} = \mathscr{E}\{R_{b_k}\}$, R_{b_k} is the up-link rate of user k, and $\hat{R}_{e_j,k} = \max \mathscr{E}\{R_{e_j,k}\}$, $R_{e_j,k}$ is the rate at eavesdropper j.

In the following sections, we analyze the ergodic secrecy rate of this model with different RIS-types: passive, active, and EH-RIS under phase shift errors. Then, a clear comparative analysis and design insights of the three RIS schemes are provided. Next, we design the phase shifts of these RIS configurations, and we present the RIS configuration selection scheme.

III. PASSIVE RIS

In this Section, we consider the case when the RIS is passive. As we have mentioned earlier, passive RIS reflects the users messages constructively to the BS with passive elements. Thus, the received signal at the BS can be expressed as

$$\mathbf{y}_b = \sum_{i=1}^{K} \sqrt{p_i L_{u_i,b}} \mathbf{G} \tilde{\Theta} \mathbf{h}_{r,i} x_i + \mathbf{n}_b \quad (5)$$

where $L_{u_i,b} = d_{u_i,r}^{-\alpha_r} d_{r,b}^{-\alpha_b}$ is the large scale fading, $d_{u_i,r}$ is the distance between user i and RIS, $d_{r,b}$ is the distance between RIS and the BS, α_r and α_b are the path-loss exponents, x_i is user i signal with unit variance, $\mathbf{n}_b$ is the additive wight Gaussian noise (AWGN) at the BS, $\mathbf{n}_b \sim CN(0, \sigma_b^2 \mathbf{I})$, $\tilde{\Theta} = \bar{\Theta}\Theta$ where $\Theta = \operatorname{diag}(\theta)$, and $\theta = [\theta_1, \ldots, \theta_M]^T$ is the RIS reflection coefficients with $\theta_m = e^{j\varphi_m}$, where $\varphi_m \in [0, 2\pi)$ is the phase shift of element m. However, in practical systems, phase shift errors can exist due to imperfect channel knowledge and finite precision in phase adjustment. Thus, we define $\bar{\Theta} = [e^{j\bar{\varphi}_1}, \ldots, e^{j\bar{\varphi}_M}]$ as the phase-shift errors at the RIS. The phase-error is

modeled according to Von-Mises (VM) distribution with zero-mean and a characteristic function (CF) $E\left[e^{j\bar{\varphi}_m}\right] = \frac{I_1(\kappa)}{I_0(\kappa)} = \rho(\kappa)$, where κ is the concentration parameter and I_i is the modified Bessel function of the first kind and order i. By applying the receive beamforming vector $\mathbf{w}_k$ at the BS, the received signal of user k is

$$\mathbf{y}_{b,k} = \sqrt{p_k L_{u_k,b}} \mathbf{w}_k \mathbf{G} \bar{\Theta}\Theta \mathbf{h}_{r,k} x_k +$$

$$\sum_{\substack{i=1 \\ i \neq k}}^{K} \sqrt{p_i L_{u_i,b}} \mathbf{w}_k \mathbf{G} \bar{\Theta}\Theta \mathbf{h}_{r,i} x_i + \mathbf{w}_k \mathbf{n}_b. \quad (6)$$

On the other hand, the received signal at eavesdropper j to detect user k signal is

$$y_{e_j,k} = \sqrt{p_k} x_k \left(\sqrt{d_{e_j,k}^{-\alpha_e}} h_{e_j,k} + \sqrt{L_{u_k,e_j}} \mathbf{h}_{e_j,r} \bar{\Theta}\Theta \mathbf{h}_{r,k} \right)$$

$$+ \sum_{\substack{i=1 \\ i \neq k}}^{K} \sqrt{p_i} x_i \left(\sqrt{d_{e_j,i}^{-\alpha_e}} h_{e_j,i} + \sum_{\substack{i=1 \\ i \neq k}}^{K} \sqrt{L_{u_i,e_j}} \mathbf{h}_{e_j,r} \bar{\Theta}\Theta \mathbf{h}_{r,i} \right)$$

$$+ n_{e_j} \quad (7)$$

where $d_{e_j,k}^{-\alpha_e}$ is the distance between user k and eavesdropper j, α_e is the path-loss exponent, $L_{u_k,B} = d_{u_k,r}^{-\alpha_r} d_{e_j,r}^{-\alpha_e}$ and $d_{e_j,r}^{-\alpha_e}$ denotes the distance between the RIS and eavesdropper j.

To calculate the ergodic secrecy rate, the ergodic up-link rate for user k and ergodic rate at the eavesdropper j should be derived, which will be considered in the following subsections.

A. Ergodic Up-link rate of user k

To calculate the ergodic user rate, maximum ratio combining (MRC) is adopted at the BS. The beamforming matrix is given by $\mathbf{W} = (\mathbf{G}\Theta\mathbf{H})^H$, and thus $\mathbf{w}_k = \mathbf{h}_{r,k}^H \Theta^H \mathbf{G}^H$. The signal to interference plus noise ratio (SINR) at the BS to decode user k signal can be written as in (8), shown at the top of next page.

Lemma 1. *The ergodic up-link rate of user k in passive RIS-aided MU-MISO systems under Rician fading channels and with phase shift error can be calculated by*

$$\mathscr{E}\{R_{b_k}\} \approx \log_2 \left(1 + \frac{p_k L_{u_k,b} \xi_k}{\sum_{\substack{i=1 \\ i \neq k}}^{K} p_i L_{u_i,b} \varsigma_i + v_k \sigma_b^2} \right) \quad (9)$$

where

$$\xi_k = \mathscr{E}\left\{ \left| \mathbf{h}_{r,k}^H \Theta^H \mathbf{G}^H \mathbf{G} \bar{\Theta}\Theta \mathbf{h}_{r,k} \right|^2 \right\} =$$

$$\gamma_{b_k} = \frac{p_k \, L_{u_k,b} \left| \mathbf{h}_{r,k}^H \Theta^H \mathbf{G}^H \mathbf{G}\Theta\bar{\Theta}\mathbf{h}_{r,k} \right|^2}{\sum\limits_{\substack{i=1 \\ i\neq k}}^{K} p_i \, L_{u_i,b} \left| \mathbf{h}_{r,k}^H \Theta^H \mathbf{G}^H \mathbf{G}\Theta\bar{\Theta}\mathbf{h}_{r,i} \right|^2 + \left\| \mathbf{h}_{r,k}^H \Theta^H \mathbf{G}^H \right\|^2 \sigma_b^2}. \tag{8}$$

$$\frac{1}{\left(\rho_b+1\right)^2 \left(\rho_k+1\right)^2} \left(a_1 N^2 + a_2 NM^2 + a_3 NM + a_4 N \right)$$

$a_1 = \Big(\rho\left(\kappa\right)^2 \left(\rho_k + \rho_b + 1\right)^2 +$
$\left(1 - \rho\left(\kappa\right)^2 \right) \rho_k \rho_b^2 + \rho_b^2 \Big) M^2$
$+ \Big(\big(\left(2\rho_k + 3\rho_b + 2 - \rho_k\rho_b\right) \rho\left(\kappa\right)^2 + \left(1+\rho_k\right)\rho_b \big)$
$\rho_b\rho_k \left|f_k\right|^2 + \left(\rho_k + \rho_b + 2\right)^2 - \rho\left(\kappa\right)^2 \left(\rho_k + \rho_b + 1\right)^2$
$-2\rho\left(\kappa\right)^2 \rho_k\rho_b - 2 \Big) M$
$+ \rho\left(\kappa\right)^2 \rho_b^2\rho_k^2 \left|f_k\right|^4 + 2 \Big(\left(1 - \rho\left(\kappa\right)^2\right)\left(\rho_k + \rho_b\right) + 2 \Big)$
$\rho_b\rho_k \left|f_k\right|^2,$
$a_2 = \Big(\rho\left(\kappa\right)^2 \rho_k\rho_b \left(1+\rho_k\right) M^2 \Big) + \left(\rho_k + \rho_b + 1\right) \rho_b\rho_r$
$+ \left(\rho_k + \rho_b + 1\right)^2 - \left(\rho_k + 1\right) \rho_b^2,$
$a_3 = \Big(\big(\left(\rho_k + 1\right) \rho\left(\kappa\right)^2 \big) + \left(\rho_k + 1\right) \Big) \rho_b\rho_k \left|f_k\right|^2$
$-2\rho_b\rho_k\rho\left(\kappa\right)^2 + 2\rho_b\rho_k + 2\rho_k + 2\rho_b - 1,$
$a_4 = 2\rho_b\rho_r \left|f_k\right|^2 \left(1 + \rho\left(\kappa\right)^2\right)$
and

$$\varsigma_i = \mathscr{E}\left\{ \left| \mathbf{h}_{r,k}^H \Theta^H \mathbf{G}^H \mathbf{G}\Theta\bar{\Theta}\mathbf{h}_{r,i} \right|^2 \right\} =$$

$$\frac{1}{\left(\rho_b+1\right)^2 \left(\rho_k+1\right)\left(\rho_i+1\right)} \left(b_1 N^2 + b_2 NM^2 + b_3 NM \right)$$

$b_1 = \Big(\rho_i + 1 - \rho\left(\kappa\right)^2 \rho_i \Big) M^2 \rho_b^2$
$+ M \Big(\big(\rho_i + 1 - \rho\left(\kappa\right)^2 \rho_i \big) \rho_b^2 \rho_k \left|f_k\right|^2 + \rho\left(\kappa\right)^2 \rho_b^2 \rho_i \left|f_i\right|^2$
$+ \left(\rho_k + 2\rho_b + 1\right)\left(\rho_i + 1 - \rho\left(\kappa\right)^2 \rho_i\right) + \rho\left(\kappa\right)^2 \rho_i \big) +$
$\Big(2\rho_b \left|f_i\right|^2 + \rho_k \left|\bar{\mathbf{h}}_k^H \bar{\mathbf{h}}_i\right|^2 + 2\rho_b\rho_k Re\left(f_k^* f_i \bar{\mathbf{h}}_i^H \bar{\mathbf{h}}_k\right) \Big)$
$\rho\left(\kappa\right)^2 \rho_i + \Big(\rho\left(\kappa\right)^2 \rho_b\rho_i \left|f_i\right|^2 + 2\rho_i \left(1 - \rho\left(\kappa\right)^2\right) + 2 \Big)$
$\rho_b\rho_k \left|f_k\right|^2,$
$b_2 = \Big(\left(\rho_b + 1\right)\rho_k + \left(\rho_b + 1\right)^2 - \rho_b^2 \Big)\left(\rho_i + 1\right)$
$- \left(\rho_b + 1\right) \rho_b\rho_i\rho\left(\kappa\right)^2 - 1$
$b_3 = \left(\rho_i + 1\right)\rho_b\rho_k \left|f_k\right|^2 + \left(\rho_k + 1\right)\rho\left(\kappa\right)^2 \rho_b\rho_i \left|f_i\right|^2$
and

$$\upsilon_k = \mathscr{E}\left\{ \left\| \mathbf{h}_{r,k}^H \Theta^H \mathbf{G}^H \right\|^2 \right\} =$$

$$\frac{L_{u_k,b}}{\left(\rho_b+1\right)\left(\rho_k+1\right)} \left(\rho_b\rho_k \left|f_k\right|^2 + \left(\rho_b + \rho_k + 1\right) M \right)$$

Proof: The proof is provided in Appendix A. ∎

B. Ergodic Rate at Eavesdropper j

The SINR at eavesdropper j to decode user k signal can be expressed as

$$\gamma_{e_j,k} = \frac{p_k \left| d_{u_k,r}^{-\frac{\alpha_r}{2}} d_{e_j,r}^{-\frac{\alpha_e}{2}} \mathbf{h}_{e_j,r}\Theta\bar{\Theta}\mathbf{h}_{r,k} + d_{e_j,k}^{-\frac{\alpha_e}{2}} h_{e_j,k} \right|^2}{\sum\limits_{\substack{i=1 \\ i\neq k}}^{K} p_i \left| d_{u_i,r}^{-\frac{\alpha_r}{2}} d_{e_j,r}^{-\frac{\alpha_e}{2}} \mathbf{h}_{e_j,r}\Theta\bar{\Theta}\mathbf{h}_{r,i} + d_{e_j,i}^{-\frac{\alpha_e}{2}} h_{e_j,i} \right|^2 + \sigma_{e_j}^2}. \tag{10}$$

Lemma 2. *The ergodic rate at eavesdropper j in up-link passive RIS-aided MU-MISO systems under Rician fading channels and with phase shift error can be calculated by*

$$\mathscr{E}\left\{ R_{e_j,k} \right\} \approx \log_2 \left(1 + \frac{p_k \, x_k}{\sum\limits_{\substack{i=1 \\ i\neq k}}^{K} p_i \, y_i + \sigma_{e_j}^2} \right) \tag{11}$$

where
$x_k = d_{u_k,r}^{-\alpha_r} d_{e_j,r}^{-\alpha_e} \Big(\frac{\rho_{e_j}}{\rho_{e_j}+1} \frac{\rho_k}{\rho_k+1} \left(M + \rho\left(\kappa\right)^2 \xi \right) +$
$\frac{\rho_{e_j}}{\rho_{e_j}+1} \frac{1}{\rho_k+1} M + \frac{\rho_k}{\rho_k+1} \frac{1}{\rho_{e_j}+1} M + \frac{1}{\rho_{e_j}+1} \frac{1}{\rho_k+1} M \Big) + d_{e_j,r}^{-\alpha_e},$
and
$y_i = d_{u_i,r}^{-\alpha_r} d_{e_j,r}^{-\alpha_e} \Big(\frac{\rho_{e_j}}{\rho_{e_j}+1} \frac{\rho_i}{\rho_i+1} \left(M + \rho\left(\kappa\right)^2 \xi \right) +$
$\frac{\rho_{e_j}}{\rho_{e_j}+1} \frac{1}{\rho_i+1} M + \frac{\rho_i}{\rho_i+1} \frac{1}{\rho_{e_j}+1} M + \frac{1}{\rho_{e_j}+1} \frac{1}{\rho_i+1} M + d_{e_j,i}^{-\alpha_e} \Big).$

Proof: Due to the paper length limitation, the proof has been omitted in this paper, and presented in Appendix B in [41]. ∎

Finally, the ergodic secrecy rate in passive RIS scheme is presented in the next theorem.

Theorem 1. *The ergodic secrecy rate in passive RIS-aided MU-MISO systems under Rician fading channels and with phase shift error can be calculated by*

$$\hat{R}_s = \left[\log_2 \left(1 + \frac{p_k \, L_{u_k,b}\xi_k}{\sum\limits_{\substack{i=1 \\ i\neq k}}^{K} p_i \, L_{u_i,b}\varsigma_i + \upsilon_k\sigma_b^2} \right) - \log_2 \left(1 + \frac{p_k \, x_k}{\sum\limits_{\substack{i=1 \\ i\neq k}}^{K} p_i \, y_i + \sigma_{e_j}^2} \right) \right]^+. \tag{12}$$

This article has been accepted for publication in IEEE Transactions on Wireless Communications. This is the author's version which has not been fully edited and content may change prior to final publication. Citation information: DOI 10.1109/TWC.2023.3340977

6

IV. ACTIVE RIS

Here we consider the case when the RIS is active. As we mentioned earlier, active RIS can adjust the phase shifts and also amplify the reflected signal to compensate the attenuation from the first link with extra power consumption. The signal reflected by the active RIS can be written as

$$\mathbf{y}_r = \tilde{\Theta} \sum_{i=1}^{K} \sqrt{p_i \, d_{u_i,r}^{-\alpha_r}} \mathbf{h}_{r,i} x_i + \tilde{\Theta}\mathbf{n}_r \qquad (13)$$

where $\mathbf{n}_r$ is the noise at RIS elements. Note that, the noise introduced at the active RIS is classified into dynamic noise and static noise [42]. The dynamic noise is introduced and amplified by the reflection-type amplifier. Whilst, the static noise is introduced by the phase-shift circuit, and it is negligible compared to the dynamic noise, as it has been verified by experimental results in [42, Section VII-A]. Thus, following [42] we neglect the static noise, and model the noise at RIS elements as $\mathbf{n}_r \sim CN\left(0, \sigma_r^2 \mathbf{I}\right)$. In this case $\tilde{\Theta} = \bar{\Theta}\Theta$ where $\Theta = \text{diag}(\theta)$, and $\theta = [\theta_1, ..., \theta_M]^T$ with $\theta_m = \varrho_m e^{j\varphi_m}$, $\varrho_m > 1$ and $\varphi_m \in [0, 2\pi)$ represents the amplification factor and phase shift coefficient, respectively, at element m. For simplicity, we assume that $\varrho_m = \varrho$ and then define $\Theta = \varrho\,\text{diag}\left\{e^{j\varphi_1}, ..., e^{j\varphi_M}\right\}$. The active RIS amplification power can be expressed as

$$P_r = \left(\sum_{i=1}^{K} \frac{p_i}{d_{u_i,r}^{\alpha_r}} \mathscr{E}\left\{\left\|\tilde{\Theta}\mathbf{h}_{r,i}\right\|^2\right\} + \mathscr{E}\left\{\left\|\tilde{\Theta}\mathbf{n}_r\right\|^2\right\}\right)$$

$$= \left(\sum_{i=1}^{K} \frac{p_i}{d_{u_i,r}^{\alpha_r}} M\varrho^2 + M\varrho^2\sigma_r^2\right) \qquad (14)$$

where $\mathscr{E}\left\|\tilde{\Theta}\mathbf{n}_r\right\|^2 = M\varrho^2\sigma_r^2$, and $\mathscr{E}\left\|\tilde{\Theta}\mathbf{h}_{r,i}\right\|^2 = \frac{\varrho^2}{\rho_i+1}\left(\rho_i\mathscr{E}\left(\bar{\mathbf{h}}_{r,i}^H\bar{\mathbf{h}}_{r,i}\right) + \mathscr{E}\left(\tilde{\mathbf{h}}_{r,i}^H\tilde{\mathbf{h}}_{r,i}\right)\right) = \frac{\varrho^2}{\rho_i+1}(\rho_i M + M) = M\varrho^2$. Thus, the amplification factor for each element on the active RIS is given by

$$\varrho = \sqrt{\frac{P_r}{M\left(\sum_{i=1}^{K} \frac{p_i}{d_{u_i,r}^{\alpha_r}} + \sigma_r^2\right)}}. \qquad (15)$$

By applying the receive beamforming vector $\mathbf{w}_k$ at the BS, the received signal of user k is

$$y_{b,k} = \sqrt{p_k \, L_{u_k,b}}\mathbf{w}_k\mathbf{G}\bar{\Theta}\Theta\mathbf{h}_{r,k}x_k$$

$$+ \sum_{\substack{i=1 \\ i\neq k}}^{K} \sqrt{p_i \, L_{u_i,b}}\mathbf{w}_k\mathbf{G}\bar{\Theta}\Theta\mathbf{h}_{r,i}x_i$$

$$+ \sqrt{d_{r,b}^{-\alpha_r}}\mathbf{w}_k\mathbf{G}\bar{\Theta}\Theta\mathbf{n}_r + \mathbf{w}_k\mathbf{n}_b. \qquad (16)$$

On the other hand, the received signal at eavesdropper j to detect user k signal is

$$y_{e_j,k} = \sqrt{p_k}x_k\left(\sqrt{d_{e_j,k}^{-\alpha_e}}h_{e_j,k} + \sqrt{L_{u_k,e_j}}\mathbf{h}_{e_j,r}\bar{\Theta}\Theta\mathbf{h}_{r,k}\right)$$

$$+ \sum_{\substack{i=1 \\ i\neq k}}^{K} \sqrt{p_i}x_i\left(\sqrt{d_{e_j,i}^{-\alpha_e}}h_{e_j,i} + \sum_{\substack{i=1 \\ i\neq k}}^{K} \sqrt{L_{u_i,e_j}}\mathbf{h}_{e_j,r}\bar{\Theta}\Theta\mathbf{h}_{r,i}\right)$$

$$+ \sqrt{d_{e_j,r}^{-\alpha_e}}\mathbf{h}_{e_j,r}\bar{\Theta}\Theta\mathbf{n}_r + n_{e_j}. \qquad (17)$$

A. Ergodic Up-link rate of user k

Applying MRC beamforming at the BS, the SINRs at the BS to decode user k signal can be expressed as as in (18), shown at the top of next page.

Lemma 3. *The ergodic up-link rate of user k in active RIS-aided MU-MISO systems under Rician fading channels and with phase shift error can be calculated by*

$$\mathscr{E}\left\{R_{b_k}\right\} \approx \log_2\left(1+\right.$$

$$\left.\frac{p_k \, L_{u_k,b}\xi_k\varrho^4}{\sum_{\substack{i=1 \\ i\neq k}}^{K} p_i \, L_{u_i,b}\varsigma_i\varrho^4 + \varrho^4 d_{r,b}^{-\alpha_r}\sigma_r^2\nu_k + \varrho^2 \upsilon_k\sigma_b^2}\right) \qquad (19)$$

where

$$\nu_k = \mathscr{E}\left\|\mathbf{h}_{r,k}^H\Theta^H\mathbf{G}^H\mathbf{G}\bar{\Theta}\Theta\right\|^2 = \frac{1}{(\rho_b+1)\sqrt{(\rho_k+1)}}(X_1 + X_2) \qquad (20)$$

and $X_1 = \mathscr{E}\left\{|\Delta_{1,1}|^2\right\} + \mathscr{E}\left\{|\Delta_{1,2}|^2\right\} + \mathscr{E}\left\{|\Delta_{1,3}|^2\right\} + \mathscr{E}\left\{|\Delta_{1,4}|^2\right\} + \mathscr{E}\left\{\Delta_{1,1}\Delta_{1,4}^*\right\}$

$\mathscr{E}\left\{|\Delta_{1,1}|^2\right\} = \rho_b^2\rho_k\left|a_M^H\left(\phi_{kr}^a, \phi_{kr}^e\right)\Theta^H a_M^H\left(\phi_r^a, \phi_r^e\right)a_N^H\left(\phi_b^a, \phi_b^e\right)a_N\left(\phi_b^a, \phi_b^e\right)\right|^2 \times M,$

$\mathscr{E}\left\{|\Delta_{1,2}|^2\right\} = \rho_b\rho_k\left|a_M^H\left(\phi_{kr}^a, \phi_{kr}^e\right)\Theta^H a_M\left(\phi_r^a, \phi_r^e\right)\right|^2 NM,$

$\mathscr{E}\left\{|\Delta_{1,3}|^2\right\} = \rho_b\rho_k MN\left(\rho(\kappa)^2 M + \left(1-\rho(\kappa)^2\right)M\right),$

$\mathscr{E}\left\{|\Delta_{1,4}|^2\right\} = \rho_k\left(N^2 M + NM^2\right),$

$\mathscr{E}\left\{\Delta_{1,1}\Delta_{1,4}^*\right\} = \rho_b\rho_k\left(a_M^H\left(\phi_{kr}^a, \phi_{kr}^e\right)\Theta^H 6\, a_M^H\left(\phi_r^a, \phi_r^e\right)a_N^H\left(\phi_b^a, \phi_b^e\right)a_N\left(\phi_b^a, \phi_b^e\right)\right)$
$\times\left(a_M\left(\phi_r^a, \phi_r^e\right)\Theta\right)\rho_k a_M^H\left(\phi_{kr}^a, \phi_{kr}^e\right)\Theta^H N\Theta,$

and $X_2 = \mathscr{E}\left\{|\Delta_{2,1}|^2\right\} + \mathscr{E}\left\{|\Delta_{2,2}|^2\right\} + \mathscr{E}\left\{|\Delta_{2,3}|^2\right\} + \mathscr{E}\left\{|\Delta_{2,4}|^2\right\} + \mathscr{E}\left\{\Delta_{2,1}\Delta_{2,4}^*\right\}$

$\mathscr{E}\left\{|\Delta_{2,1}|^2\right\} = \rho_b^2\left\|\Theta^H a_M^H\left(\phi_r^a, \phi_r^e\right)a_N^H\left(\phi_b^a, \phi_b^e\right)a_N\left(\phi_b^a, \phi_b^e\right)a_M\left(\phi_r^a, \phi_r^e\right)\Theta\right\|_F^2,$

$\mathscr{E}\left\{|\Delta_{2,2}|^2\right\} = \rho_b\left\|\Theta^H a_M\left(\phi_r^a, \phi_r^e\right)\right\|^2 NM,$

$\mathscr{E}\left\{|\Delta_{2,3}|^2\right\} = \rho_b MN\left(\left\|a_M^H\left(\phi_r^a, \phi_r^e\right)\Theta\bar{\Theta}\right\|^2\right) = \rho_b M^2 N,$

$\mathscr{E}\left\{|\Delta_{2,4}|^2\right\} = \rho_k^2\left(N^2 M + NM^2\right),$

This article has been accepted for publication in IEEE Transactions on Wireless Communications. This is the author's version which has not been fully edited and content may change prior to final publication. Citation information: DOI 10.1109/TWC.2023.3340977

7

$$\gamma_{b_k} = \frac{p_k L_{u_k,b} \left|\mathbf{h}_{r,k}^H \Theta^H \mathbf{G}^H \mathbf{G} \Theta \bar{\Theta} \mathbf{h}_{r,k}\right|^2}{\sum\limits_{\substack{i=1\\i\neq k}}^{K} p_i L_{u_i,b} \left|\mathbf{h}_{r,k}^H \Theta^H \mathbf{G}^H \mathbf{G} \Theta \bar{\Theta} \mathbf{h}_{r,i}\right|^2 + d_{r,b}^{-\alpha_r} \left\|\mathbf{h}_{r,k}^H \Theta^H \mathbf{G}^H \mathbf{G} \bar{\Theta} \Theta\right\|^2 \sigma_r^2 + \left\|\mathbf{h}_{r,k}^H \Theta^H \mathbf{G}^H\right\|^2 \sigma_b^2}. \tag{18}$$

$$\gamma_{e_{j,k}} = \frac{p_k \left|d_{u_k,r}^{-\frac{\alpha_r}{2}} d_{e_j,r}^{-\frac{\alpha_e}{2}} \mathbf{h}_{e_j,r} \Theta \bar{\Theta} \mathbf{h}_{r,k} + d_{e_j,k}^{-\frac{\alpha_e}{2}} h_{e_j,k}\right|^2}{\sum\limits_{\substack{i=1\\i\neq k}}^{K} p_i \left|d_{u_i,r}^{-\frac{\alpha_r}{2}} d_{e_j,r}^{-\frac{\alpha_e}{2}} \mathbf{h}_{e_j,r} \Theta \bar{\Theta} \mathbf{h}_{r,i} + d_{e_j,i}^{-\frac{\alpha_e}{2}} h_{e_j,i}\right|^2 + d_{e_j,r}^{-\alpha_e} \left\|\mathbf{h}_{e_j,r} \bar{\Theta} \Theta\right\|^2 \sigma_r^2 + \sigma_{e_j}^2}. \tag{21}$$

$\mathscr{E}\left\{\Delta_{2,1}\Delta_{2,4}^*\right\} = \rho_k \left(a_M \left(\phi_r^a, \phi_r^e\right) \Theta\right) \rho_k \Theta N \Theta^H$
$\left(\Theta^H a_M^H \left(\phi_r^a, \phi_r^e\right) a_N^H \left(\phi_b^a, \phi_b^e\right) a_N \left(\phi_b^a, \phi_b^e\right)\right).$

Proof: Due to the paper length limitation, the proof has been omitted in this paper, and presented in Appendix C in [41]. ∎

B. Ergodic Rate at Eavesdropper j

The SINR at eavesdropper j to decode user k signal in this scenario can be written as in (21) shown at the top of next page.

Lemma 4. *The ergodic rate at eavesdropper j in up-link active RIS-aided MU-MISO systems under Rician fading channels and with phase shift error can be calculated by*

$$\mathscr{E}\left\{R_{e_{j,k}}\right\} \approx \log_2\left(1 + \frac{p_k x_j}{\sum\limits_{\substack{i=1\\i\neq k}}^{K} p_i y_i + z_j \sigma_r^2 + \sigma_{e_j}^2}\right) \tag{22}$$

where
$x_j = d_{u_k,r}^{-\alpha_r} d_{e_j,r}^{-\alpha_e} \varrho^2 \left(\frac{\rho_{e_j}}{\rho_{e_j}+1}\frac{\rho_k}{\rho_k+1}\left(M + \rho(\kappa)^2 \xi\right) + \right.$
$\left. \frac{\rho_{e_j}}{\rho_{e_j}+1}\frac{1}{\rho_k+1}M + \frac{\rho_k}{\rho_k+1}\frac{1}{\rho_{e_j}+1}M + \frac{1}{\rho_{e_j}+1}\frac{1}{\rho_k+1}M\right) + d_{e_j,r}^{-\alpha_e},$
$y_k = d_{u_i,r}^{-\alpha_r} d_{e_j,r}^{-\alpha_e} \varrho^2 \left(\frac{\rho_{e_j}}{\rho_{e_j}+1}\frac{\rho_i}{\rho_i+1}\left(M + \rho(\kappa)^2 \xi\right) + \right.$
$\left. \frac{\rho_{e_j}}{\rho_{e_j}+1}\frac{1}{\rho_i+1}M + \frac{\rho_i}{\rho_i+1}\frac{1}{\rho_{e_j}+1}M + \frac{1}{\rho_{e_j}+1}\frac{1}{\rho_i+1}M + d_{e_j,i}^{-\alpha_e}\right)$
which have been derived in Appendix B in [41], and
$z_j = d_{e_j,r}^{-\alpha_e} \mathscr{E}\left\|\mathbf{h}_{e_j,r}\tilde{\Theta}\right\|^2 = $
$d_{e_j,r}^{-\alpha_e} \frac{\varrho^2}{\rho_{e_j,r}+1}\left(\rho_{e_j,r}\mathscr{E}\left(\bar{\mathbf{h}}_{e_j,r}^H \bar{\mathbf{h}}_{e_j,r}\right) + \mathscr{E}\left(\tilde{\mathbf{h}}_{e_j,r}^H \tilde{\mathbf{h}}_{e_j,r}\right)\right)$
$= d_{e_j,r}^{-\alpha_e} \frac{\varrho^2}{\rho_{e_j,r}+1}\left(\rho_{e_j,r}M + M\right) = d_{e_j,r}^{-\alpha_e} M \varrho^2.$

The ergodic secrecy rate in active RIS scheme is presented in the following Theorem.

Theorem 2. *The ergodic secrecy rate in active RIS-aided MU-MISO systems under Rician fading channels and with phase shift error can be calculated by*

$$\hat{R}_s = \left[\log_2\left(1 + \frac{p_k L_{u_k,b}\xi_k \varrho^4}{\sum\limits_{\substack{i=1\\i\neq k}}^{K} p_i L_{u_i,b}\varsigma_i \varrho^4 + \varrho^4 d_{r,b}^{-\alpha_r}\sigma_r^2 \nu_k + \varrho^2 \upsilon_k \sigma_b^2}\right) \right.$$
$$\left. - \log_2\left(1 + \frac{p_k x_j}{\sum\limits_{\substack{i=1\\i\neq k}}^{K} p_i y_i + z_j \sigma_r^2 + \sigma_{e_j}^2}\right)\right]^+. \tag{23}$$

V. EH RIS

Following the recent works in [18]–[22], in this section, we consider the case when the RIS is an energy constrained node and it can harvest RF energy to support its operation. Thus, in this scenario the whole operation time block, T, is split into two time periods, the energy transfer (ET) slot and the information transfer (IT) slot. During the ET slot, the BS transmits energy signals to the RIS to support its operation. During the IT slot, the users deliver their messages to the BS through the RIS. We denote τT as the time duration for the ET, and $(1 - \tau)T$ as the time duration for IT. The received signals at the RIS in the first sub-slot is expressed as

$$y_r = \sqrt{P_b}\mathbf{G}_p \mathbf{W}_p \mathbf{x}_p + \mathbf{n}_r \tag{24}$$

where P_b is the BS power, $\mathbf{G}_p = \left(\sqrt{\frac{\rho_p}{\rho_p+1}}\bar{\mathbf{G}}_p + \sqrt{\frac{1}{\rho_p+1}}\tilde{\mathbf{G}}_p\right)$ is the BS-RIS channel in the ET slot, $\mathbf{W}_p$ is the precoding matrix and $\mathbf{x}_p$ is the energy signals vector. Using the maximum ratio transmission (MRT) scheme, the harvested power at the RIS can be expressed as $P_r = \frac{\eta_{eff}\tau P_b \|\mathbf{G}_p\|_F^2}{1-\tau}$, which can be written as $P_r = \frac{\eta_{eff}\tau P_b \text{Tr}\left(G_b G_b^H\right)}{1-\tau}$ where η_{eff} is the efficiency of EH. Since $G_b G_b^H$ has Wishart distribution, the average harvested power can be written as

$$P_r = \frac{\eta_{eff}\tau P_b \mathscr{E}\left\{\text{Tr}\left(G_b G_b^H\right)\right\}}{1-\tau} = \frac{\eta_{eff}\tau P_b NM}{1-\tau}. \tag{25}$$

$$\gamma_{b_k} = \frac{p_k \, L_{u_k,b} \left| \mathbf{h}_{r,k}^H \Theta^H \mathbf{G}^H \mathbf{G} \Theta \bar{\Theta} \mathbf{h}_{r,k} \right|^2}{\displaystyle\sum_{\substack{i=1 \\ i \neq k}}^{K} p_i \, L_{u_i,b} \left| \mathbf{h}_{r,k}^H \Theta^H \mathbf{G}^H \mathbf{G} \Theta \bar{\Theta} \mathbf{h}_{r,i} \right|^2 + d_{r,b}^{-\alpha_r} \left\| \mathbf{h}_{r,k}^H \Theta^H \mathbf{G}^H \mathbf{G} \bar{\Theta} \Theta \right\|^2 \sigma_r^2 + \left\| \mathbf{h}_{r,k}^H \Theta^H \mathbf{G}^H \right\|^2 \sigma_b^2}. \tag{27}$$

$$\gamma_{e_{j,k}} = \frac{p_k \left| d_{u_k,r}^{-\frac{\alpha_r}{2}} d_{e_j,r}^{-\frac{\alpha_e}{2}} \mathbf{h}_{e_j,r} \Theta \bar{\Theta} \mathbf{h}_{r,k} + d_{e_j,k}^{-\frac{\alpha_e}{2}} h_{e_j,k} \right|^2}{\displaystyle\sum_{\substack{i=1 \\ i \neq k}}^{K} p_i \left| d_{u_i,r}^{-\frac{\alpha_r}{2}} d_{e_j,r}^{-\frac{\alpha_e}{2}} \mathbf{h}_{e_j,r} \Theta \bar{\Theta} \mathbf{h}_{r,i} + d_{e_j,i}^{-\frac{\alpha_e}{2}} h_{e_j,i} \right|^2 + d_{e_j,r}^{-\alpha_e} \left\| \mathbf{h}_{e_j,r} \bar{\Theta} \Theta \right\|^2 \sigma_r^2 + \sigma_{e_j}^2}. \tag{29}$$

By substituting (25) into (15), the amplification factor for each element on the RIS in this case is given by

$$\hat{\varrho} = \sqrt{\frac{\eta_{eff} \tau P_b N M}{M (1 - \tau) \left(\displaystyle\sum_{i=1}^{K} \frac{p_i}{d_{u_i,r}^{\alpha_r}} + \sigma_r^2 \right)}}. \tag{26}$$

A. Ergodic Up-link rate of user k

Applying MRC beamforming at the BS, the SINR at the BS to decode user k signal can be expressed as as in (27), shown at the top of next page.

Lemma 5. *The ergodic up-link rate of user k in EH RIS-aided MU-MISO systems under Rician fading channels and with phase shift error can be calculated by*

$$\mathscr{E} \{ R_{b_k} \} \approx (1 - \tau) \log_2 \left(1 + \right.$$

$$\left. \frac{p_k \, L_{u_k,b} \xi_k \hat{\varrho}^4}{\displaystyle\sum_{\substack{i=1 \\ i \neq k}}^{K} p_i \, L_{u_i,b} \varsigma_i \hat{\varrho}^4 + \hat{\varrho}^4 d_{r,b}^{-\alpha_r} \sigma_r^2 \nu_k + \hat{\varrho}^2 \upsilon_k \sigma_b^2} \right). \tag{28}$$

Proof: This expression can be obtained by following similar steps as in Appendix C in [41]. ∎

B. Ergodic Rate at Eavesdropper j

The SINR at eavesdropper j to decode user k signal is given by (29), shown at the top of next page.

Lemma 6. *The ergodic rate at eavesdropper j in up-link EH RIS-aided MU-MISO systems under Rician fading channels and with phase shift error can be calculated by*

$$\mathscr{E} \{ R_{e_{j,k}} \} \approx (1 - \tau) \log_2 \left(1 + \frac{p_k \, \hat{x}_j}{\displaystyle\sum_{\substack{i=1 \\ i \neq k}}^{K} p_i \hat{y}_i + \hat{z}_j \sigma_r^2 + \sigma_{e_j}^2} \right) \tag{30}$$

where

$$\hat{x}_j = d_{u_k,r}^{-\alpha_r} d_{e_j,r}^{-\alpha_e} \hat{\varrho}^2 \left(\frac{\rho_{e_j}}{\rho_{e_j}+1} \frac{\rho_k}{\rho_k+1} \left(M + \rho (\kappa)^2 \xi \right) + \frac{\rho_{e_j}}{\rho_{e_j}+1} \frac{1}{\rho_k+1} M + \frac{\rho_k}{\rho_k+1} \frac{1}{\rho_{e_j}+1} M + \frac{1}{\rho_{e_j}+1} \frac{1}{\rho_k+1} M \right) + d_{e_j,r}^{-\alpha_e},$$

$$\hat{y}_i = d_{u_i,r}^{-\alpha_r} d_{e_j,r}^{-\alpha_e} \hat{\varrho}^2 \left(\frac{\rho_{e_j}}{\rho_{e_j}+1} \frac{\rho_i}{\rho_i+1} \left(M + \rho (\kappa)^2 \xi \right) + \frac{\rho_{e_j}}{\rho_{e_j}+1} \frac{1}{\rho_i+1} M + \frac{\rho_i}{\rho_i+1} \frac{1}{\rho_{e_j}+1} M + \frac{1}{\rho_{e_j}+1} \frac{1}{\rho_i+1} M + d_{e_j,i}^{-\alpha_e} \right)$$

$$\hat{z}_j = d_{e_j,r}^{-\alpha_e} M \hat{\varrho}^2,$$

which have been derived in the previous section.

Finally, the ergodic secrecy rate in EH RIS scheme is presented in the next Theorem.

Theorem 3. *The ergodic secrecy rate of user k in EH active RIS-aided MU-MISO systems under Rician fading channels and with phase shift error can be calculated by (31), shown at the top of next page.*

VI. DISCUSSION

From the secrecy rate expressions provided in Theorems 1,2 and 3, we can observe the following insights. Firstly, the ergodic secrecy rates for Rayleigh fading channels can be obtained easily by setting all the Rician factors to zero, e.g., $\rho_b = \rho_{e_j,r} = \rho_k = 0$. Generally, in all RIS schemes, the phase shifts should be optimized to reduce the information leakage caused by the phase shift errors. In addition, the secrecy performance of the RIS schemes under phase shift errors is highly related to the total power consumption, number of the RIS elements, BS antennas, and noises at the BS and RIS.

From Theorem 1: the secrecy performance of the passive RIS depends essentially on the user power, p_k, and as the phase shift errors increase the user power should be increased. In case the users have limited power, the secrecy rate can be enhanced by increasing number of RIS units and/or BS antennas. Specifically, increasing number of BS antennas leads to improve only the ergodic rate at the BS. However, increasing number of RIS elements has an impact on the both ergodic rates at the BS and the eavesdroppers. Furthermore, the noise at the BS has been amplified by the receive beamforming (MRC) vector, and thus increasing the noise variance reduces the system security.

From Theorem 2: in active RIS the secrecy performance depends on both the user power, p_k, and also the am-

$$\hat{R}_s = \left[(1-\tau)\log_2\left(1 + \frac{p_k\, L_{u_k,b}\xi_k\hat{\varrho}^4}{\sum\limits_{\substack{i=1\\i\neq k}}^{K} p_i\, L_{u_i,b}\varsigma_i\hat{\varrho}^4 + \hat{\varrho}^4 d_{r,b}^{-\alpha_r}\sigma_r^2\nu_k + \hat{\varrho}^2 \upsilon_k\sigma_b^2}\right) - (1-\tau)\log_2\left(1 + \frac{p_k\,\hat{x}_j}{\sum\limits_{\substack{i=1\\i\neq k}}^{K} p_i\hat{y}_i + \hat{z}_j\sigma_r^2 + \sigma_{e_j}^2}\right) \right]^+ \quad (31)$$

plification factor for each RIS element, ϱ. Thus, if the users have limited power transmission, the security can be controlled by adjusting the RIS power, P_r. However, consuming power at the RIS can cause a degradation in the energy efficiency, and thus there should be a trade-off between the required secrecy rate and the total power consumption. In addition, the ergodic rates at the BS and the eavesdroppers are impacted by the amplified RIS noise, and thus high RIS noise variance can degrade the ergodic rates on both sides. Implementing more BS antennas and/or RIS elements enhance the system's security.

From Theorem 3: the secrecy performance of the EH-RIS relies also on the energy transfer time duration, τ, and the BS power P_b. Increasing the BS power increases amount of the EH at the RIS, and thus improves the secrecy rate as in the active RIS scheme. However, due to the impact of the path loss the BS might consume a large amount of power to charge the RIS and provide the required energy, and thus this scheme is not energy efficient and might be preferred in short-distance applications. In EH-RIS, number of BS antennas has an impact on both the achievable rates at the BS and the eavesdroppers. Notable, unlike the conventional passive and active RISs, to provide the best secrecy performance the EH-RIS should be located near the BS (to harvest more power) or near the users (to reduce the path loss). Finally and similar to active RIS, the amplified RIS noise power hurts the two ergodic rates.

Therefore, for given system parameters, the suitable RIS scheme can be chosen by considering the trade-off between the required secrecy rate and amount of the transmission powers in the system. This will be investigated in the next Section.

VII. System Design

In this section, based on the derived analytical expressions, we first design the phase shifts of the RIS configurations considered in this work. Then, the best RIS configuration selection scheme is presented.

A. Phase Shift Optimization

The secrecy rate expressions presented in Theorems, 1, 2 and 3, show that the secrecy performance relies on the phase shifts of the RIS elements. In this work, it is assumed that the CSI of the eavesdroppers is unknown at the BS/RIS (only channel distribution known). Therefore, to enhance the system performance, the RIS phase shifts can

be optimized by maximizing the achievable ergodic sum rate. Since the phase shift at each unit of the RIS lies in the range of $[0, 2\pi)$, the phase shift optimization problem can be formulated as

$$\max_{\Theta} \quad \sum_{i=1}^{K} \hat{R}_{b_i}$$
$$s.t \quad \varphi_m \in [0, 2\pi), \quad \vee m. \quad (32)$$

where the phase shifts are continuous values in the range of $\varphi_m \in [0, 2\pi)$. In case the phase shifts vary in a discrete range, the phase shifts constraint in (32) becomes in the form, $\varphi_m \in \left[0, \frac{2\pi}{2^B}, 2 \times \frac{2\pi}{2^B}, ..., \left(2^B - 1\right)\frac{2\pi}{2^B},\right) \vee m$, where the range is divided into B bits, thus the phase shifts are more accurate with a larger B value. Due to the complicated formula of the ergodic sum rate, it is difficult to optimize (32) based on the conventional techniques. However, GA-based methods can be employed to solve this optimization problem. Due to the page limitation, we refer readers to [6] for more details about the GA methods. The efficiency of the GA in optimizing the RIS phase shifts has been widely verified in the literature [5], [6], [25], [26], [43].

As an efficient suboptimal solution, the RIS phase shifts can be aligned to user k, who transmits the confidential message. This presents a simple sub-optimal solution for enhancing the secrecy rate [6]. Accordingly, the phase shifts should be

$$\varphi_m = -2\pi\frac{d}{\lambda}\left(x_m t_k + y_m l_k\right),$$

$$t_k = \sin\phi_{kr}^a \sin\phi_{kr}^e - \sin\phi_t^a \sin\phi_t^e, l_k = \cos\phi_{kr}^e - \cos\phi_t^e. \quad (33)$$

B. RIS Configuration Selection Scheme

In this Section, based on the required secrecy rate (r_s) and amount of the power available at the users, and the RIS, we propose a configuration selection scheme which can be used to select the best system configuration, i.e., passive RIS, active RIS or EH RIS. The proposed RIS configuration selection scheme can help the network designers to select the best RIS-type that can provide secure communication. In addition, it can also be used in hybrid-RIS schemes where the reflecting units can be switched into different modes flexibly [44]. Also, in hybrid-RIS schemes, in which

This article has been accepted for publication in IEEE Transactions on Wireless Communications. This is the author's version which has not been fully edited and content may change prior to final publication. Citation information: DOI 10.1109/TWC.2023.3340977

10

the BS is connected with different RIS types [45]. It is worth mentioning that, the analysis in this work and the RIS configuration selection scheme are based on different power statuses at the users.

A) If user k has sufficient amount of power to achieve the target secrecy rate, in this case passive RIS can be implemented. Based on the secrecy rate expression provided in Theorem 1, the required user k power, p_k, to achieve the target secrecy rate, r_s, can be obtained by solving

$$
\begin{aligned}
r_s =\ & \log_2\left(1 + \frac{p_k\,L_{u_k,b}\xi_k}{\sum\limits_{\substack{i=1\\i\neq k}}^{K} p_i\,L_{u_i,b}\varsigma_i + \upsilon_k\sigma_b^2}\right) \\
& - \log_2\left(1 + \frac{p_k\,x_k}{\sum\limits_{\substack{i=1\\i\neq k}}^{K} p_i\,y_i + \sigma_{e_j}^2}\right)
\end{aligned} \tag{34}
$$

which can be found as function of other users powers $p_i, i \in [1,K], i \neq k$ as

$$
p_k = \frac{p_1 - p_2}{p_3 - p_4} \tag{35}
$$

where $p_1 = \dfrac{\sum\limits_{\substack{i=1\\i\neq k}}^{K} p_i\,L_{u_i,b}\varsigma_i + \upsilon_k\sigma_b^2}{\sum\limits_{\substack{i=1\\i\neq k}}^{K} p_i\,L_{u_i,b}\varsigma_i + \upsilon_k\sigma_b^2}$, $p_2 = \dfrac{2^{r_s}\sum\limits_{\substack{i=1\\i\neq k}}^{K} p_i\,y_i + 2^{r_s}\sigma_{e_j}^2}{\sum\limits_{\substack{i=1\\i\neq k}}^{K} p_i\,y_i + \sigma_{e_j}^2}$,

$p_3 = \dfrac{2^{r_s}\,x_k}{\sum\limits_{\substack{i=1\\i\neq k}}^{K} p_i\,y_i + \sigma_{e_j}^2}$ and $p_4 = \dfrac{L_{u_k,b}\xi_k}{\sum\limits_{\substack{i=1\\i\neq k}}^{K} p_i\,L_{u_i,b}\varsigma_i + \upsilon_k\sigma_b^2}$.

B) If user k has limited amount of power, e.g., the user power, p_k, is less than the power required in (35). In this case active RIS can be implemented to provide the target secrecy rate. Based on the secrecy rate expression provided in Theorem 2, the required RIS power, ϱ or P_r, to achieve the target secrecy rate, r_s, can be obtained as function of the users powers $p_i, i \in [1,K]$ by solving

$$
\begin{aligned}
r_s =\ & \log_2\left(1 + \frac{p_k\,L_{u_k,b}\xi_k\varrho^2}{\sum\limits_{\substack{i=1\\i\neq k}}^{K} p_i\,L_{u_i,b}\varsigma_i\varrho^2 + \varrho^2 d_{r,b}^{-\alpha_r}\sigma_r^2\nu_k + \upsilon_k\sigma_b^2}\right) \\
& - \log_2\left(1 + \frac{p_k\varrho^2 x_1 + p_k x_2}{\sum\limits_{\substack{i=1\\i\neq k}}^{K} p_i\varrho^2 y_{1i} + \sum\limits_{\substack{i=1\\i\neq k}}^{K} p_i y_{2i} + z_1\varrho^2\sigma_r^2 + \sigma_{e_j}^2}\right)
\end{aligned} \tag{36}
$$

where

$$
x_1 = d_{u_k,r}^{-\alpha_r}d_{e_j,r}^{-\alpha_e}\left(\frac{\rho_{e_j}}{\rho_{e_j}+1}\frac{\rho_k}{\rho_k+1}\left(M+\rho(\kappa)^2\xi\right)+\right.
$$
$$
\left.\frac{\rho_{e_j}}{\rho_{e_j}+1}\frac{1}{\rho_k+1}M+\frac{\rho_k}{\rho_k+1}\frac{1}{\rho_{e_j}+1}M+\frac{1}{\rho_{e_j}+1}\frac{1}{\rho_k+1}M\right), \quad x_2 =
$$
$$
d_{e_j,r}^{-\alpha_e},
$$
$$
y_{1i} = d_{u_i,r}^{-\alpha_r}d_{e_j,r}^{-\alpha_e}\left(\frac{\rho_{e_j}}{\rho_{e_j}+1}\frac{\rho_i}{\rho_i+1}\left(M+\rho(\kappa)^2\xi\right)+\right.
$$
$$
\left.\frac{\rho_{e_j}}{\rho_{e_j}+1}\frac{1}{\rho_i+1}M+\frac{\rho_i}{\rho_i+1}\frac{1}{\rho_{e_j}+1}M+\frac{1}{\rho_{e_j}+1}\frac{1}{\rho_i+1}M\right), \quad y_{2i} =
$$
$$
d_{e_j,i}^{-\alpha_e},
$$

and $z_1 = d_{e_j,r}^{-\alpha_e}M$. After some simplifications, the last equation can be expressed as

$$
\varrho^4(q_1-q_3)+\varrho^2(q_2-q_4-q_5+q_7)+(q_8-q_6)=0 \tag{37}
$$

where

$$
q_1 = \sum_{\substack{i=1\\i\neq k}}^{K} p_i\,L_{u_i,b}\varsigma_i \sum_{\substack{i=1\\i\neq k}}^{K} p_i y_{1i} + d_{r,b}^{-\alpha_r}\sigma_r^2\nu_k \sum_{\substack{i=1\\i\neq k}}^{K} p_i y_{1i} + \sum_{\substack{i=1\\i\neq k}}^{K}
$$
$$
p_i\,L_{u_i,b}\varsigma_i z_1\sigma_r^2 + d_{r,b}^{-\alpha_r}\sigma_r^2\nu_k z_1\sigma_r^2 + \sum_{\substack{i=1\\i\neq k}}^{K} p_i\,L_{u_i,b}\varsigma_i p_k x_1 +
$$
$$
d_{r,b}^{-\alpha_r}\sigma_r^2\nu_k p_k x_1,
$$

$$
q_2 = \left(\upsilon_k\sigma_b^2 \sum_{\substack{i=1\\i\neq k}}^{K} p_i y_{1i} + \upsilon_k\sigma_b^2 z_1\sigma_r^2 + \upsilon_k\sigma_b^2 p_k x_1\right),
$$

$$
q_3 = \sum_{\substack{i=1\\i\neq k}}^{K} p_i y_{1i} p_k\,L_{u_k,b}\xi_k + z_1\sigma_r^2 p_k\,L_{u_k,b}\xi_k + \sum_{\substack{i=1\\i\neq k}}^{K}
$$
$$
p_i y_{1i} \sum_{\substack{i=1\\i\neq k}}^{K} p_i\,L_{u_i,b}\varsigma_i + z_1\sigma_r^2 \sum_{\substack{i=1\\i\neq k}}^{K} p_i\,L_{u_i,b}\varsigma_i + \sum_{\substack{i=1\\i\neq k}}^{K}
$$
$$
p_i y_{1i} d_{r,b}^{-\alpha_r}\sigma_r^2\nu_k + z_1\sigma_r^2 d_{r,b}^{-\alpha_r}\sigma_r^2\nu_k,
$$

$$
q_4 = \sum_{\substack{i=1\\i\neq k}}^{K} p_i y_{2i} p_k\,L_{u_k,b}\xi_k + \sigma_{e_j}^2 p_k\,L_{u_k,b}\xi_k + \sum_{\substack{i=1\\i\neq k}}^{K} p_i y_{2i} \sum_{\substack{i=1\\i\neq k}}^{K}
$$
$$
p_i\,L_{u_i,b}\varsigma_i + \sigma_{e_j}^2 \sum_{\substack{i=1\\i\neq k}}^{K} p_i\,L_{u_i,b}\varsigma_i + \sum_{\substack{i=1\\i\neq k}}^{K} p_i y_{2i} d_{r,b}^{-\alpha_r}\sigma_r^2\nu_k +
$$
$$
\sigma_{e_j}^2 d_{r,b}^{-\alpha_r}\sigma_r^2\nu_k,
$$

$$
q_5 = \left(\sum_{\substack{i=1\\i\neq k}}^{K} p_i y_{1i}\upsilon_k\sigma_b^2 + z_1\sigma_r^2\upsilon_k\sigma_b^2\right), \quad q_6 = \sum_{\substack{i=1\\i\neq k}}^{K}
$$
$$
p_i y_{2i}\upsilon_k\sigma_b^2 + \sigma_{e_j}^2\upsilon_k\sigma_b^2,
$$

$$
q_7 = \sum_{\substack{i=1\\i\neq k}}^{K} p_i\,L_{u_i,b}\varsigma_i\varrho^2 2^{r_s}p_k x_2 +
$$
$$
\varrho^2 d_{r,b}^{-\alpha_r}\sigma_r^2\nu_k 2^{r_s}p_k x_2 + \sum_{\substack{i=1\\i\neq k}}^{K} p_i\,L_{u_i,b}\varsigma_i 2^{r_s}\sigma_{e_j}^2 +
$$
$$
d_{r,b}^{-\alpha_r}\sigma_r^2\nu_k 2^{r_s}\sigma_{e_j}^2 + \sum_{\substack{i=1\\i\neq k}}^{K} p_i\,L_{u_i,b}\varsigma_i 2^{r_s} \sum_{\substack{i=1\\i\neq k}}^{K} p_i y_{2i} +
$$
$$
d_{r,b}^{-\alpha_r}\sigma_r^2\nu_k 2^{r_s} \sum_{\substack{i=1\\i\neq k}}^{K} p_i y_{2i},
$$

$$
q_8 = \upsilon_k\sigma_b^2 2^{r_s}p_k x_2 + \upsilon_k\sigma_b^2 2^{r_s}\sigma_{e_j}^2 + \upsilon_k\sigma_b^2 2^{r_s} \sum_{\substack{i=1\\i\neq k}}^{K} p_i y_{2i}.
$$

Thus, from (15), the RIS power should be higher than or equal to (38), shown at the top of next page.

$$P_r = M \left(\frac{-\left(q_2 - q_4 - q_5 + q_7\right) \pm \sqrt{\left(q_2 - q_4 - q_5 + q_7\right)^2 - 4\left(q_1 - q_3\right)\left(q_8 - q_6\right)}}{2\left(q_1 - q_3\right)} \right) \left(\sum_{i=1}^{K} \frac{p_i}{d_{u_i,r}^{\alpha_r}} + \sigma_r^2 \right). \tag{38}$$

$$P_b = \frac{M\left(1 - \tau\right)}{\eta_{eff}\tau NM} \left(\frac{-\left(q_2 - q_4 - q_5 + q_7\right) \pm \sqrt{\left(q_2 - q_4 - q_5 + q_7\right)^2 - 4\left(q_1 - q_3\right)\left(q_8 - q_6\right)}}{2\left(q_1 - q_3\right)} \right)$$

$$\times \left(\sum_{i=1}^{K} \frac{p_i}{d_{u_i,r}^{\alpha_r}} + \sigma_r^2 \right). \tag{39}$$

C) If user k and the RIS have limited amount of power, e,g., user k power, p_k, is less than the required power in (35) and the RIS power, P_r, is less than the required power in (38). In this case EH RIS can be implemented to provide the target secrecy rate. Based on (25) and (38), the required BS power, P_b, to charge the RIS and achieve the target secrecy rate, r_s, can be obtained as function of the users powers $p_i, i \in [1, K]$ by (39), shown at the top of next page.

VIII. Numerical Results

In this section, we present simulation and numerical results to assess the accuracy of the derived expressions and the secrecy performance of the RIS schemes considered in this paper. Monte-Carlo simulations with 10^5 independent trials are executed. The locations of the BS and the RIS are (0 m, 0 m), (20 m, 20 m), respectively, while the users are scattered on the corners of a square. Specifically, the coordinates for the users square are (30 m, 5 m), (35 m, 5 m), (30 m,–5 m), and (35 m,–5 m), respectively, while the eavesdroppers are distributed in a circle centered at (20 m, 0 m) with radius of 10 m [46]. Unless otherwise specified, the simulation settings are assumed as follows: $K = J = 4$, $N = 10$, $M = 5$, the users power $p_i = 2$W, the active RIS power $P_r = 7$W , the BS power in EH RIS scenario $P_b = 50$W, $B = 6$, and the nodes have same noise variance, $\sigma^2 = -70$ dBm [46]. In addition, the path-loss exponent is 2.7, the Rician factors $\rho = 0.5$. The values of the AoA and AoD of the BS and the RIS are uni-formally distributed in $(0, 2\pi)$, and the concentration parameter of RIS phase error $\kappa = 2$.

Firstly, in Fig. 2, we illustrate the ergodic secrecy rate versus the transmission user power, p_k, for the three considered RIS schemes. Fig. 2a shows the secrecy rate with phase shift errors and Fig. 2b, presents the secrecy rate for the ideal scenario when there is no phase error at RIS. Additionally in these results, we present the secrecy performance of the EH RIS scheme for different BS power $P_b = 7$W and 50W. It is clear from this figure that the analytical results are in good agreement with the simulated results, which confirms the validity of the analysis presented in this paper. It is also evident that for the given parameters' values, the secrecy rate loss due to the imperfect phase shift at the RIS is

about 0.75 bits/s/Hz. In addition, the passive RIS achieves the lowest secrecy rate, but with the smallest amount of power consumption. The secrecy rate gain of the active RIS above the passive RIS is about 0.8 bits/s/Hz for a given user power, but with extra power consumption which is around 7W. Furthermore, in the EH RIS when $P_b = 7$W, the EH RIS has lower secrecy performance than the active RIS due to the path loss in the EH phase. However, the EH RIS outperforms the active RIS when the BS consumes high transmission power $P_b = 50$W. In the EH RIS, the BS can control the secrecy performance by adjusting the transmission power in the EH phase. EH RSI scheme can be used in case the active RIS is unable to achieve the required secrecy rate, thus it is very efficient/beneficial in practical scenarios where the active RIS is not easily accessible to increase/change its battery.

To demonstrate the impact of the RIS location on the secrecy performance of the three RIS configuration schemes, in Fig. 3, we plot the secrecy rate versus the x-coordinate of the RIS $(x_{RIS}$m$)$ when $K = 4$ and $K = 2$. Several interesting observations can be extracted from these results. Firstly, in the passive and active RIS schemes the secrecy performance is worst when the RIS is located close to the BS, $x_{RIS} = 5$m, or after the users, $x_{RIS} > 35$m, due to the impact of the path-loss. In addition, there exists only one optimal location for the RIS which is around 25m. Thus, in passive and active RIS schemes, different from the conventional RIS deployment, the RIS should be deployed close to the users to achieve better secrecy performance [47], [48]. On the other hand, the EH-RIS scheme achieves better secrecy performance when the RIS is located either near the BS or the users. This is because when the BS is close to the BS amount of the harvested power at the EH-RIS will be high enough to achieve secure communication, while installing the EH-RIS close to the users can reduce the impact of the path loss. Finally, the secrecy rate deteriorates when number of the users, K, is high, due to an increase in the interference power.

Fig. 4, depicts the secrecy rate versus the user power, p_k, for different optimization schemes GA and exhaustive search methods, when $K = 2$, and $M = 3$. It is interesting to observe that the GA-scheme achieves almost the same
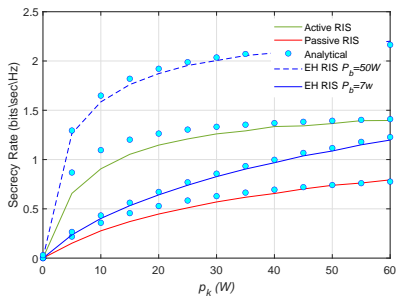
(a) Secrecy rate versus user, k, power with phase shift error.
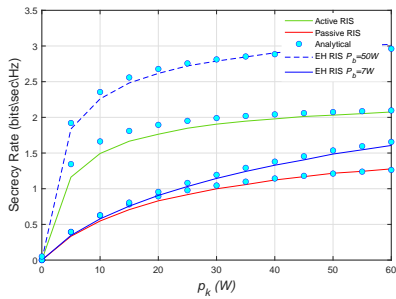
(b) Secrecy rate versus user, k, power with no phase shift error.

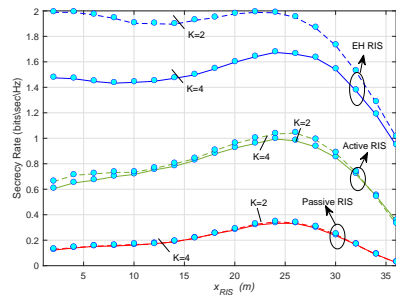Figure 2: Secrecy rate versus user, k, power with and without phase shift error.

Figure 3: Secrecy rate versus the location of the RIS, where the RIS is located at $(x_{RIS}, 20m)$.

Figure 4: Secrecy rate versus user, k, power for different optimization schemes.
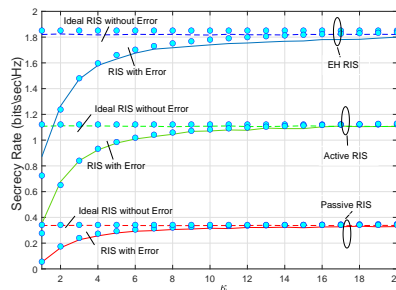
Figure 5: Secrecy rate versus concentration parameter, κ, of RIS phase error.

secrecy rate as the globally optimal solution attained by the exhaustive search scheme. These results confirm the efficiency of the GA approach to obtain the optimal RIS phase shifts, which has been verified in the literature [5], [6], [25], [26], [43].

To explain the impact of the phase errors at the RIS on the secrecy performance, in Fig. 5, we plot the secrecy rate versus the concentration parameter of the phase error, κ. Additionally, the results of ideal RIS are also presented in this figure. It can be observed from these results that the secrecy rate enhances as the concentration parameter, κ, increases. In addition, at high concentration parameter values, $\kappa \longrightarrow \infty$, the secrecy rate achieved by imperfect RIS saturates to that achieved by ideal RIS. This can be explained by the fact that the phase error at the RIS is assumed to follow a Von Mises distribution, thus high
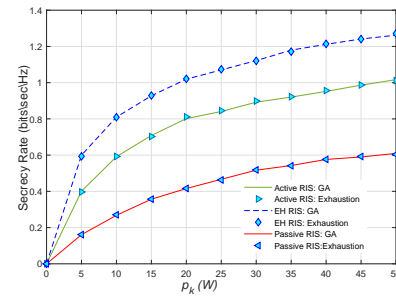
concentration parameter values make the error fluctuate in a smaller range, and when $\kappa \longrightarrow \infty$, the error at the RIS tends to zero. Accordingly, the secrecy rate of imperfect RIS converges to the ideal RIS case as $\kappa \longrightarrow \infty$, as explained in Fig. 5.

Furthermore, Fig. 6 shows the secrecy rate versus the number of BS antennas N for the all RIS schemes. It is evident and as expected, increasing the number of BS antennas N enhances the secrecy performance for the all RIS schemes. It should be pointed out that the number of BS antennas, N, has impact only on the received signal at the BS, thus increasing N results in enhancing the rate of the legitimate users. However N dose not have any impact on the rate at the eavesdroppers. Having said that in EH RIS, increasing N also increases the amount of the harvested energy at the RIS. Thus, in EH RIS, N has impact on both achievable rates at the BS and the eavesdroppers.

In Fig. 7, we depict the secrecy rate versus the number of RIS elements, M, for the all considered RIS schemes. To obtain clear insights and results, in this figure the noise variance at the nodes is assumed to be $\sigma^2 = -20$ dBm. Notably and as expected, increasing M results in enhancing the secrecy rate for the all considered scenarios. In addition, as we can notice from the analytical expressions of the secrecy rate presented in this paper, the number of RIS elements M has impact on both the achievable rate at the BS and the eavesdroppers, e.g., adding more RIS elements increases the rate at the BS and the eavesdroppers. However this improvement in the rate is essential at the BS, because
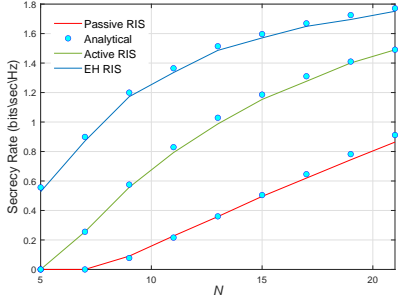
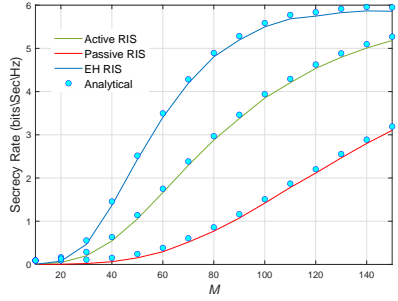Figure 6: Secrecy rate versus number of BS antennas, N, with phase shift error.

Figure 7: Secrecy rate versus number of RIS elements, M, with phase shift error.

the RIS phase shifts are designed to be toward the BS direction. It is also clear from these results that when $M > 150$ the EH RIS scheme tends to be non-increasing with M. This is because the numerator and the denominator of the SINRs at the BS and the eavesdroppers are in the same order. Thus, when number of the RIS elements is very large, $M \to \infty$, the secrecy rate will be almost fixed.

In order to illustrate the RIS configuration selection scheme, in Fig. 8 we plot the user power versus the target secrecy rate for different values of the concentration parameter of RIS phase error, $\kappa = 2$ and 8. Firstly, in Figs. 8a and 8b, we consider two examples, when the target secrecy rate is assumed to be $r_s = 0.75 \ (bits/s/Hz)$ and $r_s = 1.2 \ (bits/s/Hz)$ for $\kappa = 2$ and 8. As we can see from the results in Fig. 8a, when $r_s = 0.75 \ (bits/s/Hz)$, passive RIS can achieve the target secrecy rate with total transmission power is $P_T = p_k = 50W$, (neglecting the small amount of power consuming at passive RIS elements), and in the active RIS scheme the user transmission power can be reduced to around $p_k = 7W$ and thus the total transmission power is $P_T = p_k + P_r = 14W$, while EH RIS scheme can achieve the target secrecy rate with the smallest amount of the user power which is about $p_k = 2.95W$, but with the highest total transmission power $P_T = p_k + P_b = 52.95W$. Similar observations can be noticed from the second scenario when $r_s = 1.2 \ (bits/s/Hz)$, passive RIS achieves the target secrecy rate with the highest user power, while EH RIS achieves, r_s, with the smallest user power but with very high total consumption power, and

the active RIS scheme works between these two regions. In addition, the concentration parameter of RIS phase error, κ, has essential impact on the required user power. By comparing Figs 8a and 8b, one can notice that as κ increases the required user power to achieve the target secrecy rate decreases. For instance when the target secrecy rate is $r_s = 0.75 \ (bits/s/Hz)$, the required user power in the passive RIS scheme is about 50W when $\kappa = 2$, and 20W when $\kappa = 8$. This is due to the fact explained in Fig. 5.

Then, in Figs. 8c and 8d, we present the RIS configuration selection scheme when the available user power is $p_k = 20W$ for $\kappa = 2$ and 8. In the first case when $\kappa = 2$, if the target secrecy rate is $r_s \le 0.45 \ (bits/s/Hz)$, passive RIS can be selected, and active RIS can be implemented if the target secrecy rate is $r_s \le 1.17 \ (bits/s/Hz)$, while EH RIS can be selected if $r_s \le 1.87 \ (bits/s/Hz)$. These secrecy rate regions of the RIS schemes become wider as the concentration parameter of RIS phase error, κ, increases. In Fig. 8d when $\kappa = 8$, passive RIS can be selected to achieve secrecy rates up to $r_s \le 0.77 \ (bits/s/Hz)$, and active RIS can be selected to perform secrecy rates less than or equal to $r_s \le 1.635 \ (bits/s/Hz)$, whilst EH RIS can be used to achieve secrecy rates up to $r_s \le 2.48 \ (bits/s/Hz)$.

IX. CONCLUSIONS

In this paper the impact of phase shift error on the secrecy performance of up-link RIS-aided MU-MISO systems was considered. Under Rician fading channels and phase shift errors the ergodic secrecy rate for, passive RIS, active RIS, and EH RIS have been analyzed. Then, the phase shifts at the RIS have been optimized based on the derived rate expressions. In addition, according to the target secrecy rate and amount of power available at the users, the best RIS configuration selection scheme has been considered. The results presented in this work demonstrated that an active RIS scheme can enhance the secrecy performance of imperfect RIS elements, especially when the users have limited amount of power. Furthermore, increasing the number of BS antennas, the concentration parameter of RIS phase error, and the number of RIS elements lead to the enhancement of the secrecy performance.

APPENDIX A

By using Jensen inequality, the ergodic rate can be expressed as in (40), shown at the top of this page. Due to the paper length limitation, in this Appendix we will explain how to calculate the average of the first term, similarly and by following similar steps we can find the average of the other terms. The first term is

$$\mathscr{E}\left\{P_k \, L_{u_k,b} \left|\mathbf{h}_{r,k}^H \Theta^H \mathbf{G}^H \mathbf{G} \Theta \bar{\Theta} \mathbf{h}_{r,k}\right|^2\right\} =$$

$$P_k \, L_{u_k,b} \mathscr{E}\left\{\left|\mathbf{h}_{r,k}^H \Theta^H \mathbf{G}^H \mathbf{G} \Theta \bar{\Theta} \mathbf{h}_{r,k}\right|^2\right\} \quad (41)$$
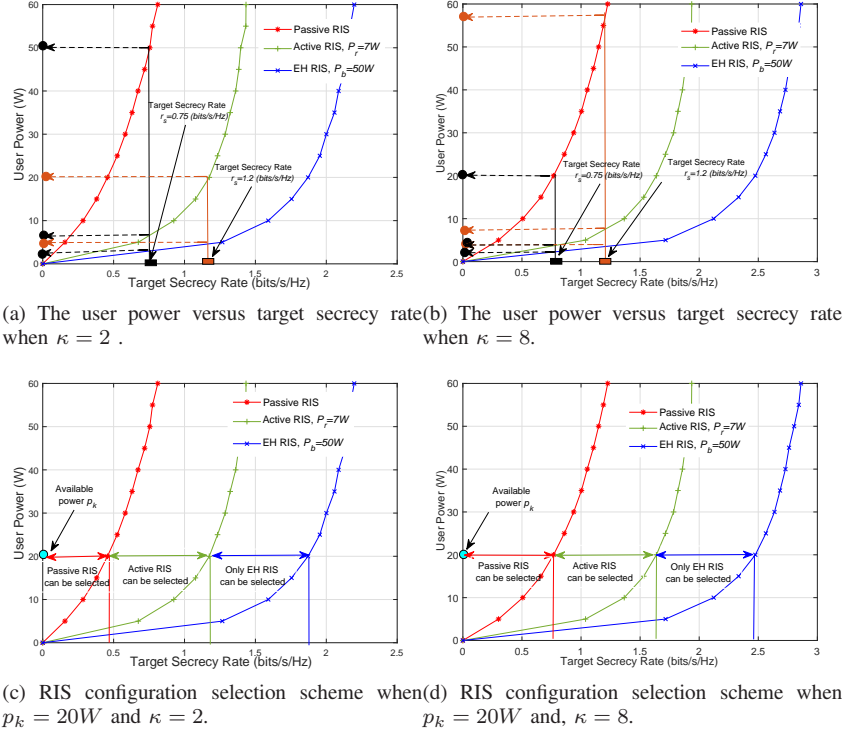
This term can be written as

(a) The user power versus target secrecy rate when $\kappa = 2$.

(b) The user power versus target secrecy rate when $\kappa = 8$.

(c) RIS configuration selection scheme when $p_k = 20W$ and $\kappa = 2$.

(d) RIS configuration selection scheme when $p_k = 20W$ and, $\kappa = 8$.

Figure 8: The user power versus target secrecy rate for different values of the concentration parameter of RIS phase error, κ.

$$\mathscr{E}\left\{R_{b_k}\right\} \approx \log_2\left(1 + \mathscr{E}\left\{\frac{p_k L_{u_{k,b}}\left|\mathbf{h}_{r,k}^H\Theta^H\mathbf{G}^H\mathbf{G}\Theta\bar{\Theta}\mathbf{h}_{r,k}\right|^2}{\sum\limits_{\substack{i=1\\i\neq k}}^{K} p_i L_{u_{i,b}}\left|\mathbf{h}_{r,k}^H\Theta^H\mathbf{G}^H\mathbf{G}\Theta\bar{\Theta}\mathbf{h}_{r,i}\right|^2 + \left\|\mathbf{h}_{r,k}^H\Theta^H\mathbf{G}^H\right\|^2\sigma_b^2}\right\}\right). \tag{40}$$

$$\mathbf{h}_{r,k}^H\Theta^H\mathbf{G}^H\mathbf{G}\Theta\bar{\Theta}\mathbf{h}_{r,k} = \frac{1}{\rho_b + 1}\mathbf{h}_{r,k}^H\mathbf{A}\bar{\Theta}\mathbf{h}_{r,k} \tag{42}$$

where
$$\mathbf{A} = \Theta^H\left(\rho_b\bar{\mathbf{G}}^H\bar{\mathbf{G}} + \sqrt{\rho_b}\bar{\mathbf{G}}^H\tilde{\mathbf{G}} + \sqrt{\rho_b}\tilde{\mathbf{G}}^H\bar{\mathbf{G}} + \tilde{\mathbf{G}}^H\tilde{\mathbf{G}}\right)\Theta.$$
Now (42) can be expressed as

$$\mathbf{h}_{r,k}^H\Theta^H\mathbf{G}^H\mathbf{G}\Theta\bar{\Theta}\mathbf{h}_{r,k} = \frac{1}{(\rho_b+1)(\rho_k+1)}$$

$$\left(\underbrace{\rho_k\bar{\mathbf{h}}_{r,k}^H\mathbf{A}\bar{\Theta}\bar{\mathbf{h}}_{r,k}}_{\Delta_1} + \underbrace{\sqrt{\rho_k}\bar{\mathbf{h}}_{r,k}^H\mathbf{A}\bar{\Theta}\tilde{\mathbf{h}}_{r,k}}_{\Delta_2}\right.$$

$$\left.+\underbrace{\sqrt{\rho_k}\tilde{\mathbf{h}}_{r,k}^H\mathbf{A}\bar{\Theta}\bar{\mathbf{h}}_{r,k}}_{\Delta_3} + \underbrace{\tilde{\mathbf{h}}_{r,k}^H\mathbf{A}\bar{\Theta}\tilde{\mathbf{h}}_{r,k}}_{\Delta_4}\right) \tag{43}$$

By removing the zero expectation terms, we can get

$$\mathscr{E}\left\{\left|\mathbf{h}_{r,k}^H\Theta^H\mathbf{G}^H\mathbf{G}\Theta\bar{\Theta}\mathbf{h}_{r,k}\right|^2\right\} =$$

$$\frac{1}{(\rho_b+1)^2(\rho_k+1)^2}\mathscr{E}\left\{\left|\sum_{i=1}^{4}\Delta_i\right|^2\right\}$$

$$= \frac{1}{(\rho_b+1)^2(\rho_k+1)^2}\left(\sum_{i=1}^{4}\mathscr{E}\left\{|\Delta_i|^2\right\} + 2\mathscr{E}\left\{\Delta_1\Delta_4^*\right\}\right) \tag{44}$$

Now the first term

$$\Delta_1 = \left(\underbrace{\rho_b\rho_k\bar{\mathbf{h}}_{r,k}^H\Theta^H\bar{\mathbf{G}}^H\bar{\mathbf{G}}\Theta\bar{\Theta}\bar{\mathbf{h}}_{r,k}}_{\Delta_{1,1}}\right.$$

$$\left.+\underbrace{\sqrt{\rho_b}\rho_k\bar{\mathbf{h}}_{r,k}^H\Theta^H\bar{\mathbf{G}}^H\tilde{\mathbf{G}}\Theta\bar{\Theta}\bar{\mathbf{h}}_{r,k}}_{\Delta_{1,2}}+\right.$$

This article has been accepted for publication in IEEE Transactions on Wireless Communications. This is the author's version which has not been fully edited and content may change prior to final publication. Citation information: DOI 10.1109/TWC.2023.3340977

15

$$\underbrace{\sqrt{\rho_b}\rho_k\bar{\mathbf{h}}_{r,k}^H\Theta^H\tilde{\mathbf{G}}^H\bar{\mathbf{G}}\Theta\bar{\Theta}\bar{\mathbf{h}}_{r,k}}_{\Delta_{1,3}} + \underbrace{\rho_k\bar{\mathbf{h}}_{r,k}^H\Theta^H\tilde{\mathbf{G}}^H\tilde{\mathbf{G}}\Theta\bar{\Theta}\bar{\mathbf{h}}_{r,k}}_{\Delta_{1,4}}\Bigg) \tag{45}$$

The average of the first term

$$\mathscr{E}\left\{|\Delta_1|^2\right\} = \mathscr{E}\left\{|\Delta_{1,1}|^2\right\} + \mathscr{E}\left\{|\Delta_{1,2}|^2\right\} +$$

$$\mathscr{E}\left\{|\Delta_{1,3}|^2\right\} + \mathscr{E}\left\{|\Delta_{1,4}|^2\right\} + 2\mathscr{E}\left\{\Delta_{1,1}\Delta_{1,4}^H\right\} \tag{46}$$

where $\Delta_{1,1} = \rho_b\rho_k\bar{\mathbf{h}}_{r,k}^H\Theta^H\bar{\mathbf{G}}^H\bar{\mathbf{G}}\Theta\bar{\Theta}\bar{\mathbf{h}}_{r,k}$, which can be written as

$$\Delta_{1,1} = \rho_b\rho_k\left(\sum_{m=1}^M a_{M,m}^H\left(\phi_{kr}^a, \phi_{kr}^e\right)e^{-j\varphi_m}a_{M,m}^H\left(\phi_r^a, \phi_r^e\right)\right)$$

$$\times\left(\sum_{m=1}^M a_{M,m}\left(\phi_{kr}^a, \phi_{kr}^e\right)e^{j\varphi_m}e^{j\bar{\varphi_m}}a_{M,m}\left(\phi_r^a, \phi_r^e\right)\right). \tag{47}$$

The average can be found as

$$\mathscr{E}\left\{|\Delta_{1,1}|^2\right\} = \rho_b^2\rho_k^2|f_k|^2\left(\left(1-\rho\left(\kappa\right)^2\right)M + \rho\left(\kappa\right)^2|f_k|^2\right) \tag{48}$$

where $f_k = \sum_{m=1}^M f_{k,m}, f_{k,m} = a_{M.m}^H\left(\phi_r^a, \phi_r^e\right)e^{j\varphi_m}a_{M,m}\left(\phi_{kr}^a, \phi_{kr}^e\right)$. The second term,

$$\Delta_{1,2} = \sqrt{\rho_b}\rho_k f_k^* \sum_{m=1}^M\sum_{n=1}^N a_{N,n}^H\left(\phi_b^a, \phi_b^e\right)$$

$$\times\tilde{\mathbf{g}}_{nm}e^{j\varphi_m}e^{j\bar{\varphi_m}}a_{M,m}\left(\phi_{kr}^a, \phi_{kr}^e\right), \tag{49}$$

$$\mathscr{E}\left\{|\Delta_{1,2}|^2\right\} = \rho_b\rho_k^2 NM|f_k|^2. \tag{50}$$

The third term

$$\Delta_{1,3} = \sqrt{\rho_b}\rho_k\sum_{m=1}^M\sum_{n=1}^N a_{N,n}^H\left(\phi_b^a, \phi_b^e\right)\tilde{g}_{nm}^H$$

$$\times e^{-j\varphi_m}a_{M,m}\left(\phi_{kr}^a, \phi_{kr}^e\right)\sum_{m=1}^M e^{j\varphi_m}f_{k,m}, \tag{51}$$

$$\mathscr{E}\left\{|\Delta_{1,3}|^2\right\} = \rho_b\rho_k^2\left(NM\rho\left(\kappa\right)^2|f_k|^2 + \left(1-\rho\left(\kappa\right)^2\right)NM^2\right). \tag{52}$$

The forth term

$$\Delta_{1,4} = \rho_k\sum_{m_1=1}^M a_{M,m_1}^H\left(\phi_{kr}^a, \phi_{kr}^e\right)e^{-j\varphi_m}\tilde{g}_{nm_1}^H$$

$$\times\sum_{m_2=1}^M \tilde{g}_{nm_2}e^{j\varphi_m}e^{j\bar{\varphi_m}}a_{M,m_2}\left(\phi_{kr}^a, \phi_{kr}^e\right), \tag{53}$$

$$\mathscr{E}\left\{|\Delta_{1,4}|^2\right\} = \rho_k NM\left(M\rho\left(\kappa\right)^2 + 1 - \rho\left(\kappa\right)^2\right) + NM^2. \tag{54}$$

The last term

$$\mathscr{E}\left\{\Delta_{1,1}\Delta_{1,4}^*\right\} = N|f_k|^2\left(M\rho\left(\kappa\right)^2 + 1 - \rho\left(\kappa\right)^2\right). \tag{55}$$

Similarly, following the same way we can find the average of the other terms.

REFERENCES

[1] M. Di Renzo, A. Zappone, M. Debbah, M.-S. Alouini, C. Yuen, J. de Rosny, and S. Tretyakov, "Smart radio environments empowered by reconfigurable intelligent surfaces: How it works, state of research, and the road ahead," *IEEE Journal on Selected Areas in Communications*, vol. 38, no. 11, pp. 2450–2525, 2020.

[2] C. Pan, H. Ren, K. Wang, J. F. Kolb, M. Elkashlan, M. Chen, M. Di Renzo, Y. Hao, J. Wang, A. L. Swindlehurst, X. You, and L. Hanzo, "Reconfigurable intelligent surfaces for 6G systems: Principles, applications, and research directions," *IEEE Communications Magazine*, vol. 59, no. 6, pp. 14–20, 2021.

[3] S. Zhang and R. Zhang, "Capacity characterization for intelligent reflecting surface aided MIMO communication," *IEEE Journal on Selected Areas in Communications*, vol. 38, no. 8, pp. 1823–1838, 2020.

[4] J. Zhang, J. Liu, S. Ma, C.-K. Wen, and S. Jin, "Large system achievable rate analysis of RIS-assisted MIMO wireless communication with statistical CSIT," *IEEE Transactions on Wireless Communications*, vol. 20, no. 9, pp. 5572–5585, 2021.

[5] K. Xu, J. Zhang, X. Yang, S. Ma, and G. Yang, "On the sum-rate of RIS-assisted MIMO multiple-access channels over spatially correlated rician fading," *IEEE Transactions on Communications*, vol. 69, no. 12, pp. 8228–8241, 2021.

[6] K. Zhi, C. Pan, H. Ren, and K. Wang, "Power scaling law analysis and phase shift optimization of RIS-aided massive MIMO systems with statistical CSI," *IEEE Transactions on Communications*, vol. 70, no. 5, pp. 3558–3574, 2022.

[7] ——, "Ergodic rate analysis of reconfigurable intelligent surface-aided massive MIMO systems with ZF detectors," *IEEE Communications Letters*, vol. 26, no. 2, pp. 264–268, 2022.

[8] ——, "Statistical CSI-based design for reconfigurable intelligent surface-aided massive MIMO systems with direct links," *IEEE Wireless Communications Letters*, vol. 10, no. 5, pp. 1128–1132, 2021.

[9] M. Abbasi Mosleh, F. Heliot, and R. Tafazolli, "Ergodic capacity analysis of reconfigurable intelligent surface assisted MIMO systems over Rayleigh-Rician channels," *IEEE Communications Letters*, pp. 1–1, 2022.

[10] W. Tang, M. Z. Chen, X. Chen, J. Y. Dai, Y. Han, M. Di Renzo, Y. Zeng, S. Jin, Q. Cheng, and T. J. Cui, "Wireless communications with reconfigurable intelligent surface: Path loss modeling and experimental measurement," *IEEE Transactions on Wireless Communications*, vol. 20, no. 1, pp. 421–439, 2021.

[11] W. Tang, X. Chen, M. Z. Chen, J. Y. Dai, Y. Han, M. D. Renzo, S. Jin, Q. Cheng, and T. J. Cui, "Path loss modeling and measurements for reconfigurable intelligent surfaces in the millimeter-wave frequency band," *IEEE Transactions on Communications*, vol. 70, no. 9, pp. 6259–6276, 2022.

[12] H. Guo, Y.-C. Liang, J. Chen, and E. G. Larsson, "Weighted sum-rate maximization for reconfigurable intelligent surface aided wireless networks," *IEEE Transactions on Wireless Communications*, vol. 19, no. 5, pp. 3064–3076, 2020.

[13] R. Long, Y.-C. Liang, Y. Pei, and E. G. Larsson, "Active reconfigurable intelligent surface-aided wireless communications," *IEEE Transactions on Wireless Communications*, vol. 20, no. 8, pp. 4962–4975, 2021.

This article has been accepted for publication in IEEE Transactions on Wireless Communications. This is the author's version which has not been fully edited and content may change prior to final publication. Citation information: DOI 10.1109/TWC.2023.3340977

16

[14] K. Zhi, C. Pan, H. Ren, K. K. Chai, and M. Elkashlan, "Active RIS versus passive RIS: Which is superior with the same power budget?" *IEEE Communications Letters*, vol. 26, no. 5, pp. 1150–1154, 2022.

[15] M. H. Khoshafa, T. M. N. Ngatched, M. H. Ahmed, and A. R. Ndjiongue, "Active reconfigurable intelligent surfaces-aided wireless communication system," *IEEE Communications Letters*, vol. 25, no. 11, pp. 3699–3703, 2021.

[16] K. Liu, Z. Zhang, L. Dai, S. Xu, and F. Yang, "Active reconfigurable intelligent surface: Fully-connected or sub-connected?" *IEEE Communications Letters*, vol. 26, no. 1, pp. 167–171, 2022.

[17] Y. Ma, M. Li, Y. Liu, Q. Wu, and Q. Liu, "Active reconfigurable intelligent surface for energy efficiency in MU-MISO systems," *IEEE Transactions on Vehicular Technology*, pp. 1–6, 2022.

[18] B. Lyu, P. Ramezani, D. T. Hoang, S. Gong, Z. Yang, and A. Jamalipour, "Optimized energy and information relaying in self-sustainable IRS-empowered WPCN," *IEEE Transactions on Communications*, vol. 69, no. 1, pp. 619–633, 2021.

[19] Y. Zou, Y. Long, S. Gong, D. T. Hoang, W. Liu, W. Cheng, and D. Niyato, "Robust beamforming optimization for self-sustainable intelligent reflecting surface assisted wireless networks," *IEEE Transactions on Cognitive Communications and Networking*, vol. 8, no. 2, pp. 856–870, 2022.

[20] Z. Chu, P. Xiao, D. Mi, W. Hao, M. Khalily, and L.-L. Yang, "A novel transmission policy for intelligent reflecting surface assisted wireless powered sensor networks," *IEEE Journal of Selected Topics in Signal Processing*, vol. 15, no. 5, pp. 1143–1158, 2021.

[21] H. Ma, H. Zhang, W. Zhang, and V. C. M. Leung, "Beamforming optimization for reconfigurable intelligent surface with power splitting aided broadcasting networks," *IEEE Transactions on Vehicular Technology*, pp. 1–6, 2022.

[22] W. Jaafar, L. Bariah, S. Muhaidat, and H. Yanikomeroglu, "Time-switching and phase-shifting control for RIS-assisted SWIPT communications," *IEEE Wireless Communications Letters*, vol. 11, no. 8, pp. 1728–1732, 2022.

[23] M.-A. Badiu and J. P. Coon, "Communication through a large reflecting surface with phase errors," *IEEE Wireless Communications Letters*, vol. 9, no. 2, pp. 184–188, 2020.

[24] D. Li, "Ergodic capacity of intelligent reflecting surface-assisted communication systems with phase errors," *IEEE Communications Letters*, vol. 24, no. 8, pp. 1646–1650, 2020.

[25] Z. Peng, X. Chen, C. Pan, M. Elkashlan, and J. Wang, "Performance analysis and optimization for RIS-assisted multi-user massive MIMO systems with imperfect hardware," *IEEE Transactions on Vehicular Technology*, vol. 71, no. 11, pp. 11 786–11 802, 2022.

[26] J. Dai, F. Zhu, C. Pan, H. Ren, and K. Wang, "Statistical CSI-based transmission design for reconfigurable intelligent surface-aided massive MIMO systems with hardware impairments," *IEEE Wireless Communications Letters*, vol. 11, no. 1, pp. 38–42, 2022.

[27] A. Papazafeiropoulos, C. Pan, P. Kourtessis, S. Chatzinotas, and J. M. Senior, "Intelligent reflecting surface-assisted MU-MISO systems with imperfect hardware: Channel estimation and beamforming design," *IEEE Transactions on Wireless Communications*, vol. 21, no. 3, pp. 2077–2092, 2022.

[28] Z. Xing, R. Wang, J. Wu, and E. Liu, "Achievable rate analysis and phase shift optimization on intelligent reflecting surface with hardware impairments," *IEEE Transactions on Wireless Communications*, vol. 20, no. 9, pp. 5514–5530, 2021.

[29] A. Salem, C. Masouros, and K.-K. Wong, "Sum rate and fairness analysis for the MU-MIMO downlink under PSK signalling: Interference suppression vs exploitation," *IEEE Transactions on Communications*, vol. 67, no. 9, pp. 6085–6098, 2019.

[30] ——, "On the secrecy performance of interference exploitation with PSK: A non-gaussian signaling analysis," *IEEE Transactions on Wireless Communications*, vol. 20, no. 11, pp. 7100–7117, 2021.

[31] A. Salem and C. Masouros, "Interference exploitation for secure communications: Error rate and secrecy analysis," in *2020 IEEE 31st Annual International Symposium on Personal, Indoor and Mobile Radio Communications*, 2020, pp. 1–6.

[32] W. Shi, Q. Wu, F. Xiao, F. Shu, and J. Wang, "Secrecy throughput maximization for IRS-aided MIMO wireless powered communication networks," *IEEE Transactions on Communications*, vol. 70, no. 11, pp. 7520–7535, 2022.

[33] L. Dong, H.-M. Wang, and J. Bai, "Active reconfigurable intelligent surface aided secure transmission," *IEEE Transactions on Vehicular Technology*, vol. 71, no. 2, pp. 2181–2186, 2022.

[34] H. Guo, Z. Yang, Y. Zou, B. Lyu, Y. Jiang, and L. Hanzo, "Joint reconfigurable intelligent surface location and passive beamforming optimization for maximizing the secrecy-rate," *IEEE Transactions on Vehicular Technology*, pp. 1–13, 2022.

[35] J. Luo, F. Wang, S. Wang, H. Wang, and D. Wang, "Reconfigurable intelligent surface: Reflection design against passive eavesdropping," *IEEE Transactions on Wireless Communications*, vol. 20, no. 5, pp. 3350–3364, 2021.

[36] J. Bai, H.-M. Wang, and P. Liu, "Robust IRS-aided secrecy transmission with location optimization," *IEEE Transactions on Communications*, vol. 70, no. 9, pp. 6149–6163, 2022.

[37] W. Lv, J. Bai, Q. Yan, and H.-M. Wang, "RIS-assisted green secure communications: Active RIS or passive RIS?" *IEEE Wireless Communications Letters*, pp. 1–1, 2022.

[38] J. D. Vega Sanchez, P. Ramirez-Espinosa, and F. J. Lopez-Martinez, "Physical layer security of large reflecting surface aided communications with phase errors," *IEEE Wireless Communications Letters*, vol. 10, no. 2, pp. 325–329, 2021.

[39] Z. Peng, Z. Zhang, L. Kong, C. Pan, L. Li, and J. Wang, "Deep reinforcement learning for RIS-aided multiuser full-duplex secure communications with hardware impairments," *IEEE Internet of Things Journal*, vol. 9, no. 21, pp. 21 121–21 135, 2022.

[40] P. Xu, G. Chen, G. Pan, and M. D. Renzo, "Ergodic secrecy rate of RIS-assisted communication systems in the presence of discrete phase shifts and multiple eavesdroppers," *IEEE Wireless Communications Letters*, vol. 10, no. 3, pp. 629–633, 2021.

[41] A. Salem, K.-K. Wong, and C.-B. Chae, "Impact of phase-shift error on the secrecy performance of uplink RIS communication systems," 2023. [Online]. Available: https://arxiv.org/abs/2301.00276

[42] Z. Zhang, L. Dai, X. Chen, C. Liu, F. Yang, R. Schober, and H. V. Poor, "Active RIS vs. passive RIS: Which will prevail in 6G?" *IEEE Transactions on Communications*, vol. 71, no. 3, pp. 1707–1725, 2023.

[43] Z. Peng, T. Li, C. Pan, H. Ren, W. Xu, and M. D. Renzo, "Analysis and optimization for RIS-aided multi-pair communications relying on statistical CSI," *IEEE Transactions on Vehicular Technology*, vol. 70, no. 4, pp. 3897–3901, 2021.

[44] H. Xie, D. Li, and B. Gu, "Exploring hybrid active-passive RIS-aided MEC systems: From the mode switching perspective," 2023.

[45] R. Liang, J. Fan, H. Liu, Y. Ge, and J. Zhang, "Dual-hop hybrid IRS-aided outdoor-to-indoor mmwave communications," *IEEE Communications Letters*, vol. 26, no. 12, pp. 2979–2983, 2022.

[46] H. Niu, Z. Chu, F. Zhou, Z. Zhu, M. Zhang, and K.-K. Wong, "Weighted sum secrecy rate maximization using intelligent reflecting surface," *IEEE Transactions on Communications*, vol. 69, no. 9, pp. 6170–6184, 2021.

[47] J. Sun, J. Li, W. Hao, X. Mu, Z. Chu, and P. Xiao, "Secure transmission design with strong channel correlation for passive/active RIS communications," *IEEE Wireless Communications Letters*, vol. 12, no. 8, pp. 1394–1398, 2023.

[48] J. Bai, H.-M. Wang, and P. Liu, "Robust IRS-aided secrecy transmission with location optimization," *IEEE Transactions on Communications*, vol. 70, no. 9, pp. 6149–6163, 2022.